Seismic and Gravity Structure of the Campi Flegrei Caldera, Italy

Francesca Bianco, Paolo Capuano, Edoardo Del Pezzo, Luca De Siena, Nils Maercklin, Guido Russo, Maurizio Vassallo, Jean Virieux, and Aldo Zollo

Abstract

We present a comprehensive review of seismic and gravity observations and tomographic models produced over the past four decades in order to understand the structure of the crust beneath the Campi Flegrei caldera. We describe the main lithological and structural discontinuities defined through these observations, illustrate their geophysical responses, and discuss the constraints they give to the understanding of magmatic and volcanic processes. Microseismic crises related to caldera unrest, and ambient seismic noise measurements provide comprehensive seismic data to local earthquake and ambient noise tomography. In combination with reflection data from onshore and offshore active seismic experiments, velocity tomography reconstructs the elastic properties of the caldera between surface and ~4 km depth. Active experiments also define the depth of lithological interfaces and deep (~7.5 km) partially molten bodies. Seismic attenuation tomography provides information complementary to velocity tomography, defining lateral lithological changes and the geometry of onshore and offshore fluid and magma bodies down to 4 km depth. Once compared with seismic analyses, gravity data highlight lateral changes in the offshore caldera structures. During the deformation and seismo-geochemical unrest (1982–1984), they permitted to reconstruct a minor (<1 km lateral extent) melt volume related to the point of maximum uplift measured at the caldera. Seismic coda-wave amplitude inversions depict the caldera rim limits in analogy to velocity tomography and map the lateral extension of ~4-km-deep deformation source. Once combined with the results from velocity tomography and gravity inversions, they reconstruct the feeding systems that connect deep deformation source and shallow vents across the eastern caldera, capped by a seismic horizon around a depth of 2 km.

F. Bianco (✉) · E. Del Pezzo
Istituto Nazionale di Geofisica e Vulcanologia, Sezione Osservatorio Vesuviano, Napoli, Italy
e-mail: francesca.bianco@ingv.it

P. Capuano
Dipartimento di Fisica "Eduardo R. Caianiello", Università di Salerno, Fisciano, SA, Italy

E. Del Pezzo
Instituto Andaluz de Geofisica, Universidad de Granada, Granada, Spain

L. De Siena
Institute of Geosciences, Johannes Gutenberg University, Mainz, Germany

N. Maercklin · G. Russo · A. Zollo
Dipartimento di Fisica, Università degli Studi di Napoli Federico II, Napoli, Italy

M. Vassallo
Istituto Nazionale di Geofisica e Vulcanologia, Sezione Roma1, Roma, Italy

J. Virieux
Institut des Science de la Terre, Université Grenoble Alpes, Grenoble, France

G. Orsi et al. (eds.), *Campi Flegrei*, Active Volcanoes of the World,
https://doi.org/10.1007/978-3-642-37060-1_2

1 Introduction

Active volcanoes undergo human-scale, time-variable ground deformation caused by both the ascent of magmas and their volatiles through the crust until eruption and the shallow circulation of hydrothermal fluids. The volcanic systems show strong heterogeneity in the physical rock properties and a large variety of non-linear thermo-mechanical processes preceding and accompanying the eruptions. Such a complexity calls for a multi-disciplinary and integrated approach for data acquisition, analysis and modelling. A reliable model of the three-dimensional distribution of the physical rock properties is necessary to understand and simulate magmatic and hydrothermal processes, including melts and fluids upwelling and eruption, and to detect and track changes in the volcanic medium properties. Such a model has been constructed for the Campi Flegrei caldera (CFc), the target volcano of this volume.

Geophysical monitoring has improved dramatically from its first steps in the 1980s (Malone et al. 1983). Since 2005, the massive deployment of digital telemetry and reliable and dense broad-band seismic networks has enabled high-quality data recording in volcanic regions, allowing an improvement in the interpretation of seismogram complexities (Hellweg 2000). This enormous technological effort has been driven by the search for increasingly refined subsurface volcano images (with spatial resolution of a few hundred meters to kilometres) mostly using local earthquake (Benz et al. 1996; Nakamichi et al. 2002; Monteiller et al. 2005; Mora et al. 2006; Patané et al. 2006) and, more recently, ambient seismic noise (Brenguier et al. 2007) tomography. The use of broad-band seismometers has opened new perspectives (Neuberg et al. 1994; Rowe et al. 1998, 2000) about the identification and physical interpretations of the large variety of typical volcanic seismic signals, such as tremors, low frequency events and tornillos, with the aim of inferring physical models of their source and relating them to underlying volcanic processes (Chouet 1988; Ferrazzini and Aki 1987; Hellweg 2000; Jousset et al. 2003; Neuberg et al. 2006). To understand volcanic processes and improve monitoring capabilities, researchers have investigated the relations between the various seismic signals and the changes in the volcano micro-scale features, such as increased heat flow or magma and hydrothermal fluids migration and chemical transformations.

Delay-time tomography of longitudinal (P) wave and shear (S) wave first-arrivals from both local micro-earthquakes and active seismic surveys is the most widely used technique to obtain subsurface images of active volcanoes (Nercessian et al. 1984, Mount Dole; Thurber 1984, Kilauea; Achauer et al. 1988, Newberry Volcano). These techniques have been extensively applied to the CFc (e.g., Battaglia et al. 2008) allowing the determination of smooth layered models. These models lack details on small interfaces, discontinuities, magma or gas accumulation zones. The velocity spatial variation mirrors the distribution of lithological and structural properties of the rocks, while the ratio between P-wave and S-wave velocities (V_P/V_S) maps rock defects, pores and cracks, and their fluid contents. Fluid-filled pores in matrix rocks result in a decrease in both V_P and V_S, while variation in V_P/V_S depends on both fluids type and pores shape (Nakajima and Hasegawa 2003; Schmeling 1985; Takei 2002).

An accurate imaging of complex, inland volcanic structures, characterised by rough topography and a highly heterogeneous propagation medium requires deeper analysis and modelling of seismograms with full waveform inversions. During the last decades, the massive data availability and the experience gained from industrial seismic exploration has led to the development and application of advanced data processing, analysis and modelling techniques to the Somma-Vesuvio volcanic system (The Internal Structure of Mount Vesuvio—TomoVes Project) and to the CFc (SEismic Reflection/Refraction Acquisition Project for Imaging complex volcanic Structures —SERAPIS project) (e.g., Gasparini et al. 1998; Zollo et al. 2003). More recently, onshore active

seismic experiments have produced extensive datasets for small volcanoes, allowing to model small-scale structures that control gas emission at the CFc (De Landro et al. 2017). These techniques permit the use of unconventional data acquisition geometries (sparse, irregular distribution of sources/receivers) and complex waveforms in the complete range of incidence angles from near-vertical to wide-angle (Auger et al. 2003; Operto et al. 2004). Both analysis and modelling of volcano seismic data have been enhanced by exploiting the whole information carried out by the direct, reflected and converted wave field through modelling of reflection amplitudes versus offset (or incidence angle). This can give important insights into the physical and lithological nature of subsurface discontinuities (Zollo et al. 2008; Maercklin and Zollo 2009). In addition, the spatial variations of both P-wave and S-wave velocity fields, as represented by tomography images, can be analysed and interpreted in terms of lithological and rheological features for rock characterisation. This interpretation can be performed by using theoretical modelling of seismic velocities in biphasic structures based on field data as well as on laboratory experiments (Vanorio et al. 2005).

The attenuation of elastic waves is quantified through the quality factor Q (the ratio between the total energy lost by a wave cycle and the energy associated with the cycle itself). Seismic attenuation tomography (Schurr et al. 2003; Nakajima and Hasegawa 2003; Hansen et al. 2004; Eberhart-Phillips et al. 2005; De Gori et al. 2005; De Siena et al. 2014a, b; Prudencio et al. 2015) has shown significant sensitivity to fluid reservoir and melt bodies at the CFc once interpreted in combination with velocity tomography results (De Siena et al. 2014a, b, 2017a, b; Serlenga et al. 2016; Akande et al. 2019). Q depends mainly on both rock temperature and presence of fluid-permeated fractures (Eberhart-Phillips et al. 2005). In addition, as Q for P-waves (Q_P) is different from that for S-waves (Q_S), the joint measure of Q for both waves is crucial for a correct characterisation of the physical state of the rocks inside a volcano. As an example, Q_p^{-1} can be used to discriminate between water-filled media and gas reservoirs (Hansen et al. 2004), while high Q_S^{-1} are a strong clue for the presence of melt-filled inclusions, which are always characterised by high V_P/V_S values (Takei 2002). Ambiguous interpretations of the causes of seismic velocity anomalies can be overcome by interpreting them jointly with the measures of Q_p^{-1} and Q_S^{-1} (De Siena et al. 2009, 2010, 2014a, b).

Scattering transfers the high-frequency energy of direct P-waves and S-waves into the coda of the seismograms (Sato et al. 2012). Due to anelasticity (seismic energy lost through heat) and scattering, the total quality factor (QT) can be separated in an anelastic part (intrinsic-Q, Qi) and in a scattering part (scattering-Q, Qsc) (Sato et al. 2012) as

$$QT = Qi \cdot Qsc/(Qi + Qsc)$$

It is challenging to separate scattering attenuation from intrinsic dissipation in single path estimates, necessary for 3D imaging (Del Pezzo et al. 2006). This is a limit for unequivocal interpretations of attenuation imaging, as the focussing-defocussing effects become indistinguishable from the scattering attenuation effects (De Siena et al. 2014b). An alternative is the use of seismic coda waves, which comprise energy scattered by direct waves in the heterogeneous volcanic medium. Both single scattering tomography (Tramelli et al. 2006) and diffusive coda imaging (De Siena et al. 2017a; Akande et al. 2019) have complemented direct wave velocity and attenuation imaging at the caldera. Scattering is also a primary ingredient in ambient noise tomography in volcanoes (Brenguier et al. 2007). This technique has provided the first onshore structural image of the CFc after the 1982–1984 unrest (De Siena et al. 2018).

Non-seismic geophysical methods help to better recognise volcano characteristics, complementing the information from seismic data and providing an integrated, more robust structural picture. Gravity investigations offer images of rock density distribution inside the Earth (e.g., Thorpe et al. 1981; Campos Enriquez and Arredondo-Fragosso 1992; Locke et al. 1993; Gailler et al. 2009; Yokoyama and Mena 1991;

Sanders et al. 1995; Davy and Caldwell 1998; Masturyono et al. 2001). If repeated through time, the study of the gravity field provides information on the evolution of the volcanic structure (e.g., Rymer 1994; Yokoyama 1989; Fournier et al. 2004). Several attempts have been made to extract useful information from gravity data collected at the CFc between 1979 and 1984 in the framework of a geothermal project and constrained by lithological information from boreholes (AGIP 1987). The data have been analysed through 2.5D modelling via the equivalent prism density method and boundary analysis (e.g., Cassano and La Torre 1987; Fedi et al. 1991; Florio et al. 1999; Berrino et al. 2008). These analyses related a gravity low centred on the town of Pozzuoli to a pyroclastic sequence with intercalated marine and continental sediments down to 2–3 km depth and overlying a thermo-metamorphic horizon. A fully 3D gravity inversion (Capuano et al. 2013) provided new insights into the internal caldera structure down to 3 km depth, defining features related to regional or volcano tectonic lineaments and dynamics. The model is parameterised on a $0.8 \times 0.8 \times 0.4$ km grid with a sequence of layers from sea bottom (0.2 km b.s.l.) down to 3 km b.s.l. with 0.4 km spacing, besides the subaerial and sea layers.

The CFc is one of the Neapolitan volcanoes that include the Somma-Vesuvio volcanic complex and the Ischia and Procida volcanic fields. All these volcanoes are located in the Campanian Plain, a Plio-Pleistocene tectonic depression (Cinque et al. 1993) formed along the Tyrrhenian margin of the Southern Apennines thrust belt in response to extensional processes (e.g., Patacca et al. 1990; Jolivet et al. 2009). The Southern Apennines belt is composed of Mesozoic carbonate and Mio-Pliocene terrigenous sequences, overlain by Quaternary continental deposits generated by the general building up of the chain and an intense volcanism. The Campanian Plain includes a 2–3,000 m thick succession of continental and marine sediments intercalated with volcanic deposits. The Mesozoic carbonate sequence of the adjacent Apennines mountains downthrown during extension, forms the basement of this sedimentary succession. The basement underlying the CFc includes a carbonate sequence with top at ~3 km depth, as inferred from seismic reflection investigations (Finetti and Morelli 1974; Bruno et al. 1998). The deepest rocks bored in the area (AGIP 1987) are calc-silicate metacarbonate rocks possibly resulting from metamorphic processes involving limestones and dolostones of the Mesozoic sequence (Vanorio and Kanitpanyacharoen 2015). The metacarbonate rocks would undergo decarbonation reactions that release lime-rich fluids promoting the formation of a seismic horizon characterised by a fibril-rich, fragile matrix in the 1–2 km depth range. This shallow interface is identified as a "caprock" by rock physics investigations (Vanorio and Kanitpanyacharoen 2015) and is analogue to those developing in geothermal reservoirs, delays deformation signals and dampens seismic and electromagnetic signals (Vanorio et al. 2005; De Siena et al. 2017a, b; Calò and Tramelli 2018; Siniscalchi et al. 2019; Akande et al. 2019).

The CFc is a nested, resurgent and restless structure in the densely populated Neapolitan area (Orsi et al. 2003; Chaps. Volcanic and Deformation History of the Campi Flegrei Volcanic Field, Italy; The Urban Development of Campi Flegrei, Italy). It results from two major nested collapses occurred during the Campanian Ignimbrite (CI; ~40 ka) and the Neapolitan Yellow Tuff (NYT; ~15 ka) eruptions. After each caldera event, volcanism was concentrated within the collapsed area. Therefore, the NYT caldera is the portion still active of the entire structure (Capuano et al. 2013 and references therein). It has been the site of intense volcanism and a long-term deformation related to the resurgence of its floor (Orsi et al. 1996, 1999, 2004; Di Vito et al. 1999). The post-NYT volcanism has generated not less than 70 eruptions grouped in three epochs of activity separated by quiescence (see Orsi et al. 1992, 1996, 2004; Chap. Volcanic and Deformation History of the Campi Flegrei Volcanic Field, Italy and references therein). The last eruption occurred in AD 1538, after 3 kyrs of quiescence, and produced the Monte Nuovo tuff cone (Di Vito et al. 2016 and references therein). The long-term deformation of the NYT caldera

floor has generated a maximum net uplift of ~90 m of La Starza resurgent block (Cinque et al. 1985). This caldera is historically characterised by recurrent, large-amplitude vertical ground displacements, known as bradyseisms, consisting of subsequent episodes of uplift and subsidence (Casertano et al. 1976) accompanied by seismicity, variation of the gravity field and increase in the fumarole and thermal spring activity. These unrest events have been interpreted as transient short-term episodes within the long-term deformation related to resurgence (Orsi et al. 1999). Oliveri del Castillo and Quagliariello (1969) and Bonafede (1991) were the first to interpret and model the Campi Flegrei ground uplift events in terms of pressure and temperature perturbations in a porous fluid-saturated medium. Such a perturbation can be generated by magmatic degassing below a hydrothermal system (Chiodini et al. 2003, 2016, 2021). The subsidence has been interpreted as the effect of lateral diffusion of hydrothermal fluids after their ascent (Gaeta et al. 1998), or as the combination of their cooling and lateral diffusion (Todesco et al. 2003). The geochemical unrest has been primarily monitored at the Solfatara crater, to the east of Pozzuoli (Chiodini et al. 2021). This area is affected by secondary deformation and seismic source paired with the primary source of uplift during unrest (Amoruso et al. 2014; De Siena et al. 2017a, b; Pepe et al. 2019). Solfatara is the surface expression of a wide hydrothermal system, identified by many researchers as the primary source of recent unrest at the caldera (Chap. The Hydrothermal System of the Campi Flegrei Caldera, Italy and references therein).

The CFc is among the best-studied volcanoes in the world due to its historical and current activity, its location in a densely populated area and the consequently high potential volcanic hazard and risk (see Chap. Volcanic Hazard Assessment at the Campi Flegrei Caldera, Italy). This chapter reviews the main observations and models inferred from the analysis of massive seismic and gravity datasets collected over the past two decades, allowing for a comprehensive geophysical hypothesis on the structural setting of the crust beneath the CFc.

2 Data and Observables

2.1 Local Earthquake Seismic Data

Since 1969 the seismicity of the caldera has been monitored by a seismic network managed by the Osservatorio Vesuviano and, for a limited period of time, by the Italian Oil Company AGIP. Most of the seismicity, considering both released seismic energy and number of seismic events, has been concentrated during two main uplift episodes that occurred in 1970–1972 and 1982–1984 (Chaps. The Permanent Monitoring System of the Campi Flegrei Caldera, Italy; The Hydrothermal System of the Campi Flegrei Caldera, Italy; Historic Unrest of the Campi Flegrei Caldera, Italy). Generally, seismicity increased when the ground uplift velocity increased. Seismicity during 1970–1972 uplift episode was characterised by a $M_L = 2.5$ maximum magnitude and several seismic swarms consisting of tens of micro-earthquakes. In the 1982–1984 episode more than 10,000 micro-earthquakes were detected; about 6,000 of them had a magnitude greater than 0.1 and included about 20 events with magnitude comprised between 2.8 and the maximum recorded value of 4.2. This episode was also characterised by seismic swarms, the largest of which occurred on April 1, 1984 and produced 513 recorded events in about 6 h. From January to June 1984 the University of Wisconsin and the Osservatorio Vesuviano jointly deployed a temporary portable digital seismic network to record the intense micro-earthquake activity. The network consisted of 13 stations equipped with three-component sensors and placed in a total of about 20 inland sites. This was the first passive seismic experiment in Italy in which digital 12 bit data-loggers were used for earthquake recording. The entire earthquake dataset from that deployment has been recovered, organised in a database of three-component waveforms, and has been completely manually re-picked to avoid possible inconsistencies merging new picks and data already used in previous studies (Capuano et al. 2006). The waveform archive consists of more than 1,000

events of which about 850 recorded by more than 3 stations. Since the end of the 1982–1984 bradyseismic episode up to the end of 2005, the CFc experienced a period of seismic quiescence, interrupted only by very few earthquakes, hence this archive represents a unique collection of waveforms produced by seismic sources in the complex volcanic area that can be very useful to better understand the post-bradyseism caldera dynamics.

The picking operation of the University of Wisconsin dataset resulted in 4,583 P-phase and 3,321 S-phase picks. Data are weighted following four classes of reading accuracy from weight 0 (best) to 3 (worst). The weight assignment takes into account the reading time error to give an idea of the pick quality (picking accuracy is in the range 0.02–0.05 s for P-waves and 0.02–0.10 s for S-waves). About 80% of the P-phase picks have a weight $p \leq 1$ and 70% of the S-phase picks a weight $p \leq 2$ (Capuano et al. 2006).

2.2 Active Seismic Data

The SERAPIS project was a dense and extended marine active seismic survey carried out in the bays of Naples and Pozzuoli in September 2001, utilising offshore seismic sources, and data acquisition on the sea bottom and inland. It was aimed at providing new insight on the caldera structure and investigating its magmatic feeding system (Zollo et al. 2003). During the course of the experiment, the vessel Nadir of IFREMER, equipped with 12, 16-L airguns, produced about 5,000 shots at 125 m distances, which were recorded by an array of 72 ocean bottom seismographs (OBS) and 62 onshore three-component stations (Fig. 1). All the seismic lines were sampled at least twice using a staggered configuration, resulting in a smaller source spacing (less than 65 m). SERAPIS provided a dense 3-D seismic coverage of the Pozzuoli Bay, the coastal portion of the CFc and the western sector of the Naples Bay. The denser 2D network of 35 OBS within the Pozzuoli Bay was designed with the aim of detecting reflected and converted waves from possible shallow to deep geological discontinuities beneath the CFc.

For most analyses all SERAPIS waveforms were band-pass filtered between 5 and 15 Hz. P-wave first-arrival travel-times were manually picked on the pre-processed traces, arranged as Common Receiver Gathers (CRG). The SERAPIS dataset processing consisted in examining 300,000 OBS waveforms and 400,000 waveforms from inland stations, providing 65,000 and 25,000 P-wave first-arrival times, respectively. These travel-time data have been used to infer 3D images of the structures of the CFc and the Naples Bay (Zollo et al. 2003; Judenherc and Zollo 2004), and were also jointly inverted with travel-times from the micro-earthquake dataset to obtain both P-wave and S-wave velocity images (Battaglia et al. 2008). Manually picked reflection travel-times and amplitudes from SERAPIS data lead to a 1D structural model of main discontinuities (Zollo et al. 2008). An iterative tomographic analysis based on automatic refined picking has been proposed and developed by Satriano et al. (2008), providing a first application of automated seismic imaging techniques and a feasibility study for the continuous-time monitoring of the space–time changing volcanic structure.

Besides the SERAPIS dataset, older marine, 2D multi-channel seismic reflection data (Finetti and Morelli 1974) were reprocessed (Bruno et al. 2003), and a high-resolution multichannel seismic survey focussed on mapping the very shallow geological features was carried out in the Pozzuoli Bay in January 2008 (Sacchi et al. 2009).

2.3 Gravity Dataset

Gravity data acquired by various institutions through several surveys performed inland and offshore the CFc and its surroundings have been collected by Capuano et al. (2013) who merged measurements on the mainland (Maino and Tribalto 1971; Cassano and La Torre 1987; Servizio Geologico d'Italia unpublished data), on the nearby island of Procida (Imbò et al. 1964) and offshore in the Gulf of Naples (Berrino et al. 1998). To obtain a better data coverage in the southern part of the study region,

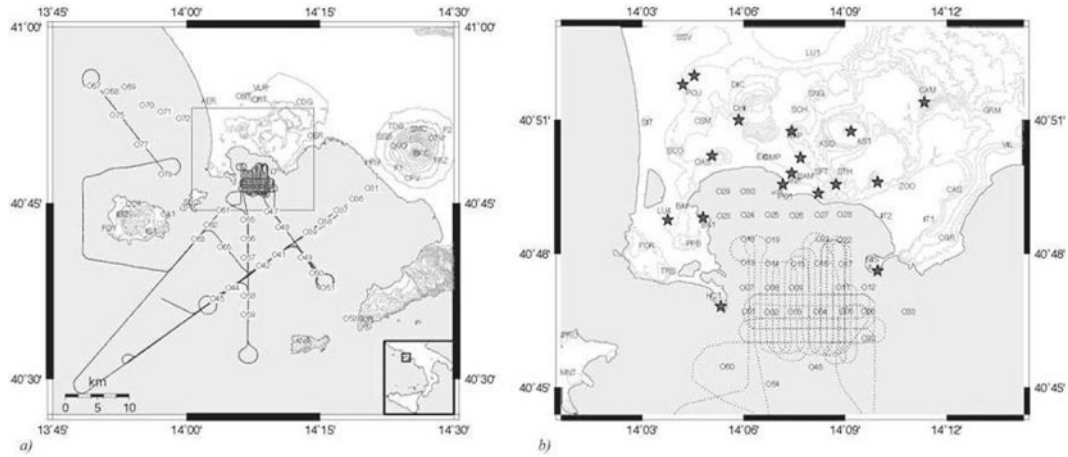

Fig. 1 **a** Map of the area investigated during the SERAPIS experiment; **b** details at Campi Flegrei. Black lines trace the path of the vessel during the survey. Dark and light circles with ID display the position of seismographs and OBS during the experiment. Stars show the locations of the UW stations deployed during 1984

the collected data were complemented with the Gravity Map of Italy. After a homogenisation process and the removal of inconsistencies, the gravity dataset consisted of 1,077 gravity measurements covering an area of about 440 km^2 (Fig. 2).

The effect of the water column and the regional gravity field were subtracted from the gravity anomaly. The sea water effect was evaluated using a large-scale bathymetric map and a water density of 1,030 kg/m^3 (Stabile et al. 2007). For the regional field correction, Capuano et al. (2013) considered that the most important regional feature of the area is the Mesozoic limestone basement that underlies the whole region at few kilometres depth. To retrieve the shape of the interface of the basement they used the results of the seismic tomography survey by Judenherc and Zollo (2004). Capuano et al. (2013) also assumed a value of 2,600 kg/m^3 for the density of the carbonate basement according to the results of other gravity investigations on the area (e.g., Cassano and La Torre 1987; Berrino et al. 2008). The local gravity anomaly used for the density inversion was obtained by subtracting all these contributions. The resulting gravity anomaly map shows a minimum associated with

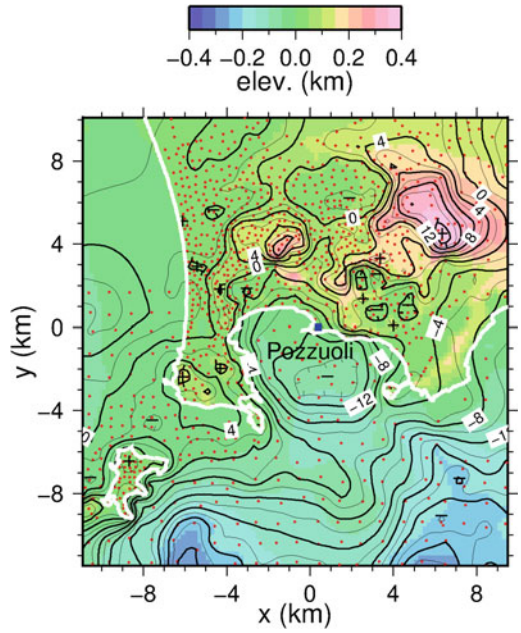

Fig. 2 Gravity anomaly map, contoured at 2 mGal intervals, obtained merging several gravity measurements datasets (see main text for details). The colour scale refers to the elevation model. Figure modified after Capuano et al. (2013)

the central portion of the CFc, together with relative maxima along its margin and in the Camaldoli area (Fig. 2).

3 The Campi Flegrei Caldera Structure Deduced by Velocity Tomography and Gravity Modelling

Since the late 1980s, the shallow crustal structure of the caldera has been investigated by several −1 to −3 km deep boreholes, local earthquake seismic tomography, gravity and magnetic surveys, as well as sporadic observations of teleseismic and wide-angle seismic data (Rosi and Sbrana 1987; Aster and Meyer 1988; Cassano and La Torre 1987; Ferrucci et al. 1992). High temperature gradients have been measured at rather shallow depths (450 °C at 3 km depth; Agip 1987). The caldera appears to be filled by a few kilometres thick sequence of volcanic and non-volcanic deposits, characterised by low V_P, high V_P/V_S and high P-wave attenuation whose geometry is consistent with the negative gravity anomaly (de Lorenzo et al. 2001). The relocated seismicity contemporaneous to the 1982–1984 ground uplift episode shows that most of the events were confined in a low-velocity layer with maximum depths of 3–4 km (Aster and Meyer 1988). The possible occurrence of a magmatic reservoir at about 4–5 km depth is based mainly on extrapolation at depth of temperature data and teleseismic observations (de Lorenzo et al. 2001; Ferrucci et al. 1992).

In the following we summarise the current knowledge on the shallow crustal structure as inferred from the results of the massive seismic velocity and gravity investigations carried out over the past two decades, referring to the 1D layered model of the CFc structure proposed by Zollo et al. (2008). In particular, we present and describe the main lithological and geological discontinuities beneath the caldera, and the geophysical characteristics of the embedded medium, from the Earth surface downward through the crust.

3.1 Shallow Unconsolidated, Water-Saturated Marine Sediments (from the Earth Surface to 900 m Depth)

Detailed information on the elastic properties of the very shallow (the uppermost kilometre) crustal structure of the CFc was mainly inferred from velocity tomography and reflection seismic analyses using SERAPIS and 2D multichannel reflection seismic datasets (Judenherc and Zollo 2004; Dello Iacono et al. 2009; Bruno et al. 2003; Sacchi et al. 2009). The subsurface of the caldera is very complex, displaying an extremely variable seismic response, especially in correspondence of the Pozzuoli Bay, where zones with excellent reflectivity and areas of a very low signal to noise ratio (S/N) alternate at relatively short distances. The signal decay is mainly due to the massive presence of volcanic rocks and edifices interlayered with Plio-Quaternary non-volcanic sediments that produce strong scattering of the seismic energy (Bruno et al. 2003). This effect is also highlighted by independent direct measurements of the separated intrinsic and scattering attenuation (Del Pezzo and Bianco 2013a). The interpreted seismic sections acquired during a multichannel seismic survey performed in the Pozzuoli Bay in January 2008, identify the well-known volcanic edifices (Pentapalummo Bank, Miseno Bank, Nisida Bank) and other buried features representing the remnant of volcanic edifices covered by marine and volcanic sediments (Sacchi et al. 2009). In such a complex environment, the determination of a velocity image of the shallow structure of the caldera requires a joint analysis of velocity tomography images and shallow seismic reflection data. This analysis was performed using an ad-hoc processing and unconventional methods applied to the data acquired within the caldera during the SERAPIS project (Zollo et al. 2003).

A refined 3D tomographic velocity model up to 1 km depth beneath the Pozzuoli Bay was obtained by the inversion of about 45,000 P-wave first-arrival travel-times, using the inversion method described in Judenherc and Zollo (2004). The obtained velocity model (Fig. 3) shows an area of low velocities (mean value of ~2,200 m/s) in the central part of the Pozzuoli Bay bordered to the south by a complex arc-shaped anomaly (Dello Iacono et al. 2009). The deeper part of the anomaly (beneath 700 m, with Vp > 3,500 m/s) correlates with rock sequences made up of agglomerate tuffs and interbedded lavas (AGIP 1987), which form the southern edge of the caldera (Barberi et al. 1991; Orsi et al. 1996). The shallower part of the anomaly that tends to split into two parallel arcs is correlated with dikes, volcanic mounds and hydrothermal alteration zones (De Bonitatibus et al. 1970; Pescatore et al. 1984; Milia and Torrente 2003). The presence of these structures suggests the existence of a highly fractured area, through which fluids (mainly gases) may have been able to rise towards the surface.

1D velocity profiles extracted from the 3D tomography model show a steep change in the P-wave velocity at about 600 m depth (Dello Iacono et al. 2009). At shallower depth, V_P values range from 1,500 to 2,000 m/s and indicate the presence of a thick, low-velocity sequence of

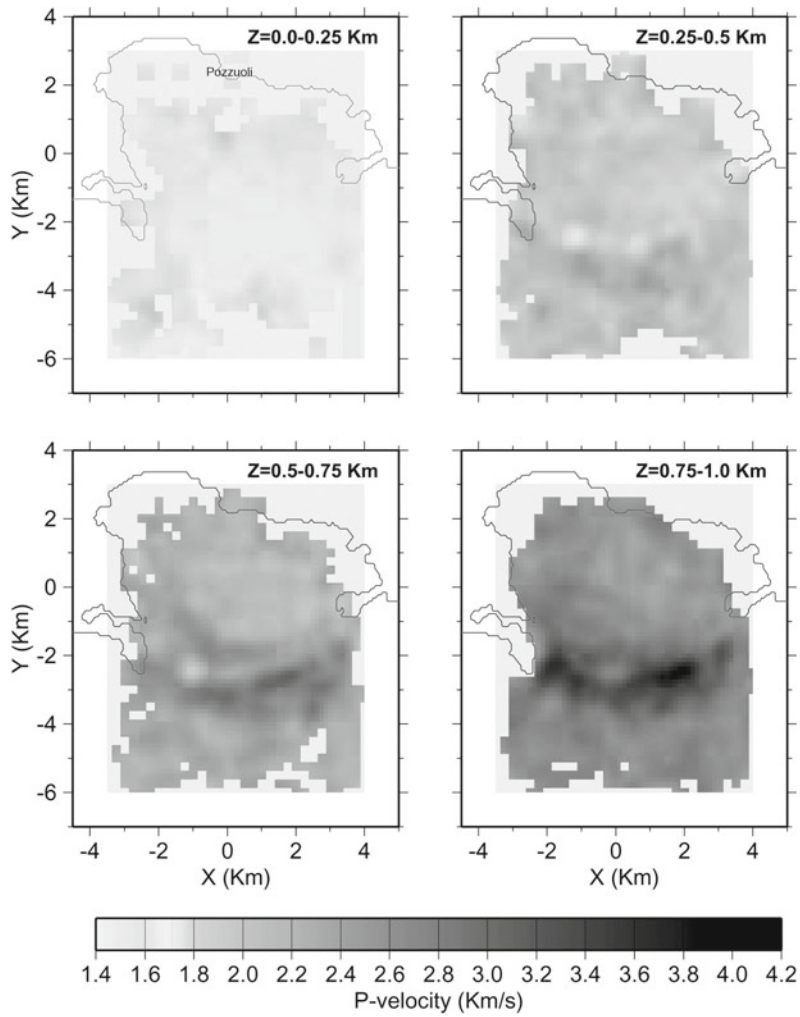

Fig. 3 Plane views of the tomography velocity model. Light grey indicates low velocities, and dark grey indicates high velocities. The top and bottom depth of each layer is indicated. Land topography is indicated by a solid line. Peripheral light grey indicates not resolved area for insufficient or absent ray coverage. Note the double-arc shaped P-wave velocity anomaly in the section 0.5–0.75 km, stretching between Nisida and Capo Miseno.
Figure modified after Dello Iacono et al. (2009)

sediments in the shallowest part of the caldera fill. In contrast, from 600 to 900 m depth, the P-wave velocity sharply increases from 2,000 to 2,600 m/s. This velocity discontinuity is also confirmed by a strong seismic reflector located at about 0.6–0.7 s two-way time on seismic sections, with data organised in Common Mid-point gathers as described in Vassallo et al. (2008). A total of 1,108 travel-time readings of P-to-P (PP) reflected waves have been manually picked on vertical-component sections corrected for a move-out velocity of 1,600 m/s. The distribution of picked travel-times has a mean value of 0.64 s with a standard deviation of 0.06 s. Assuming the mean two-way time of the PP phase as the zero-offset time for the identified reflector, and using the mean P-velocity profile inferred from the seismic tomography model of the Pozzuoli Bay area, an interface depth of 600 ± 120 m is obtained. The value of V_P/V_S ratio of the layer was computed assuming a horizontally layered subsurface model and using a maximisation of a coherency function along theoretical travel-times of P-to-S (PS) reflected phases. The theoretical travel-times were computed using the information on the propagation media extracted by the velocity tomography structure previously determined. The coherency function is computed for all Common-Midpoint gathers using the amplitudes of seismic traces in a window along the theoretical travel-times, and V_P/V_S ratio with the related uncertainty are obtained from the maximum of the coherency function (Vassallo et al. 2008). A weighted average of $V_P/V_S = 3.7 \pm 0.9$ for the shallowest layer was computed using the estimates for all Common Midpoint gathers and the inverse of the uncertainties as weighting factors. This relatively high value is an average estimate of the whole shallow layer that could be strongly influenced by the saturation conditions of the rocks in the shallowest hundreds of metres. Theoretical rock physical modelling of the V_P/V_S values as a function of porosity suggests that the shallow layer is likely formed by a sequence of incoherent, water saturated, volcanic and marine sediments that was deposited on the caldera floor (Dello Iacono et al. 2009).

A layer with such physical characteristics could have important impact on the understanding of the processes that rule the ongoing deformation of the caldera. Therefore, to test the hypothesis of a large V_P/V_S value, Dello Iacono et al. (2009) modelled the variation of the V_P/V_S ratio as a function of porosity in unconsolidated sediments, withstanding pressure conditions appropriate to describe a layer above 600 m depth. The elastic properties of the rocks depend upon the properties of the solid frame, such as composition and grain contact stiffness, and pore fluid and porosity. High V_P/V_S values are characteristic of shallow water-flow sediments at depth between 400 and 2,000 m below seabed (Huffman and Castagna 2001). At such a burial depth, these sediments are poorly consolidated (i.e., low grain contact stiffness) and withstand low effective stresses. Thus, they are near a transition between loose and consolidated rocks characterised by a critical porosity (Φc) (Nur et al. 1991, 1995). Φc separates the mechanical behaviour of rocks into two distinct domains: for porosities lower than Φc, the mineral grains are load-bearing, whereas at porosities greater than Φc, sediments fall apart and behave as a mineral-pore suspension. Dello Iacono et al. (2009) theoretically reproduced the effects of poorly consolidated sediments lying at 500 m depth on the elastic properties, via modelling as proposed by Dvorkin et al. (1999). The lower Hashin–Shtrikman bound is the tightest minimum bound possible from range of composite moduli for a two-phase material (e.g., Hashin and Shtrikman 1963; Mavko et al. 1998). It was adopted as the most appropriate model to simulate the elastic properties of these unconsolidated sediments and, therefore, looking for the softest rock arrangement. Figure 4 shows the variation of the V_P/V_S value as a function of porosity for an unconsolidated quartz-sand having a critical porosity of 38%. Figure 4a shows that the V_P/V_S value increases with increasing porosity, as in fluid-bearing sediments shear-wave velocity approaches zero while the compression-wave velocity does not fall below the velocity of a suspension of sand in water. Zimmer (2003) showed a similar trend in the V_P/V_S value

(Fig. 4b) for a set of reconstituted, unconsolidated sand and glass-bead samples under low pressure conditions. The modelling results and the experimental measurements reported for unconsolidated sediments (Zimmer 2003) suggest that the large changes predicted in the V_P/V_S value at low effective pressures are consistent with the hypothesis of poorly consolidated, fully water-saturated sediments lying above 600 m depth.

The density structure (Fig. 5) has been retrieved by inverting gravity data searching for a Tichonov regularised solution of the linear discrete inverse problem having the smallest possible weighted norm (Capuano et al. 2013). The application of regularisation theory to gravimetric and electromagnetic data is extensively discussed by Zdhanov (2002). The key point of the theory is that a stable solution of the inverse problem can be obtained requiring that the model fits the observed data within a given accuracy δ, usually linked to data and model errors. The weighting matrix associated to the model parameters is chosen to maximise the sensitivity of model parameters to data changes (Zdhanov 2002). To evaluate the goodness of the 3D density anomalies distribution at depth, the density transitions from positive to negative have been positively compared with the stratigraphic sequences drilled at Mofete and San Vito (AGIP 1987), showing that they well match the changes from tuffites and sedimentary material to lavas (flows and domes) (Rosi et al. 1983). The final gravity model obtained by Capuano et al. (2013) has a root mean square of 0.16 mGal, the misfit respect to the observed data is almost everywhere very small and the resolution is good down to

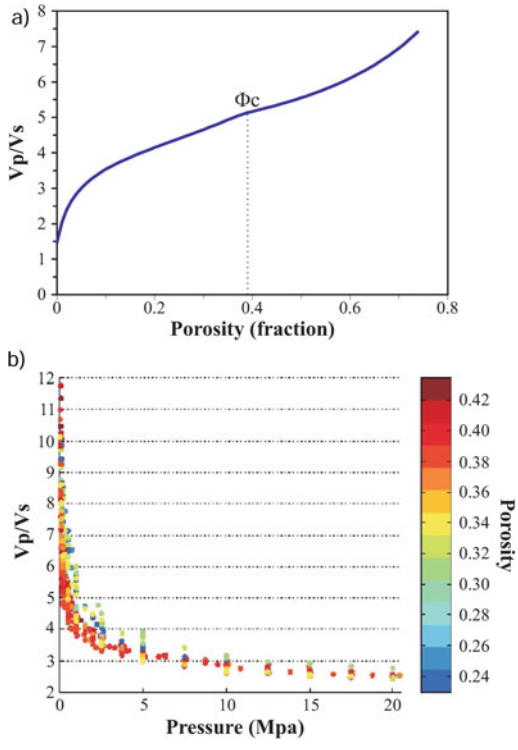

Fig. 4 **a** Variation in the V_P/V_S ratio as a function of porosity in unconsolidated, water-saturated sediments. The critical porosity is 0.38 and the number of contacts per grain is 8.5. **b** V_P/V_S ratio data for water-saturated glass-bead samples plotted against the effective pressure. Data are in colour scale as a function of porosity. Figure modified after Zimmer (2003)

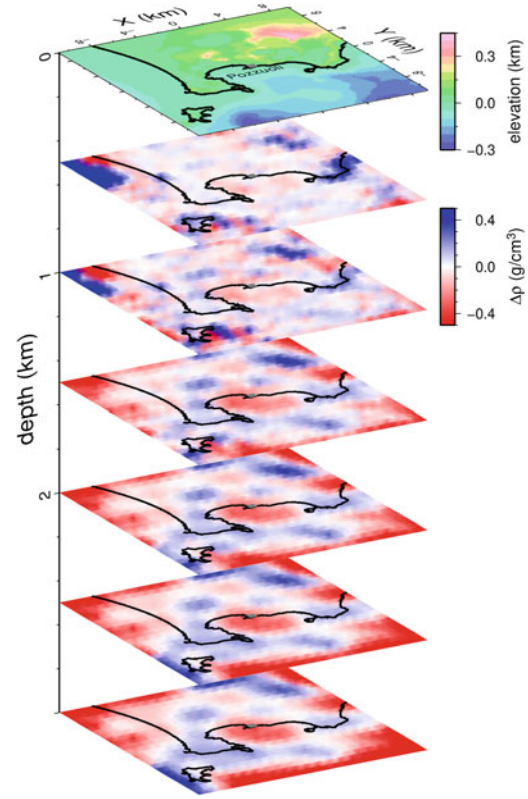

Fig. 5 3D imaging of the density model at different depths (0–3 km). The uppermost slice shows the topography. Density model after Capuano et al. (2013)

about 3 km depth. Between 0 and 200 m depth, the resulting density model is characterised by alternation of positive and negative anomalies mostly in correspondence of rock bodies of different characters (e.g., lava flows, lava domes, pyroclastic deposits). Between 200 and 600 m depth (Fig. 6) the caldera is characterised mostly by negative density anomalies. The Pozzuoli Bay morphological low is dominated by a density low about 6 km wide. Its western portion includes a large-wavelength, roughly north–south aligned and irregularly shaped structure. This density low is compatible with low velocity inferred by the seismic analysis and ascribed to the caldera fill composed of volcanic and non-volcanic sediments.

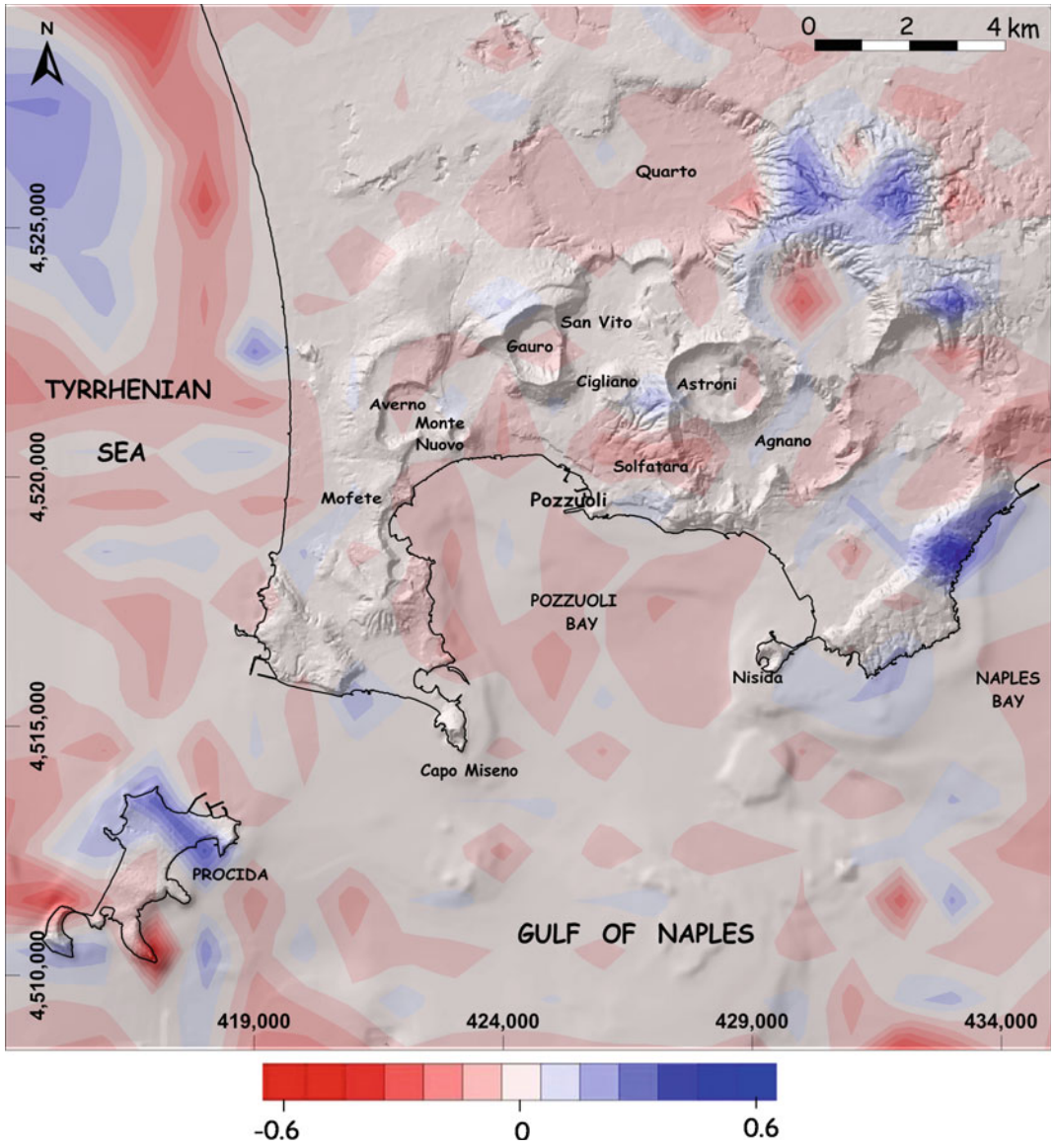

Fig. 6 Density horizontal slice between 200 and 600 m b.s.l. Colour scale represents density contrasts (g/cm^3). Figure modified after Capuano et al. (2013)

3.2 Volcanic and Non-Volcanic Deposits, Buried Caldera Rim and Fluid-/Gas-Bearing Thermometamorphic Rocks (from 500 m to ~4 km Depth)

The highest resolution seismic image of the caldera buried rim was obtained by the inversion and modelling of 77,000 arrival times of P-wave first-arrivals recorded during the SERAPIS experiment by the OBS deployed in the Pozzuoli Bay (Zollo et al. 2003). A delay-time inversion technique has been applied, based on a linearised, perturbative approach, with the use of smoothness constraint equations to regularise the solution and to stabilise the inversion procedure (Hole 1992; Benz et al. 1996).

The 3D tomography images show the presence of an arc-like, vertically-extended high P-velocity anomaly (V_P = 3.5–4.0 km/s) within the southern portion of the Pozzuoli Bay, interpreted as the expression of the caldera margin (Fig. 7). This anomaly has its top at about 800 m depth, extends to about 2,000 m depth and follows a pattern nearly concentric to the coastal line. The shape of the reconstructed caldera rim is well consistent with and closely matches the density model inferred by gravity data which have been integrated with the existing data set (Berrino et al. 1998) and re-processed by Capuano and Achauer (2003), providing with an updated Bouguer anomaly map. Litho-stratigraphic and sonic log data from several 2–3 km deep inland boreholes, drilled for geothermal exploration purposes, indicated that the caldera margin is formed by a sequence of compacted tuffs, tuffs with interbedded lavas and thermo-metamorphic rocks, with the latter at about 2–2.5 km depth. P-wave log velocities in boreholes vary with depth from 2.7–3 km/s at 0.8–1 km depth to 3.6–4.2 km/s at 2–2.2 km depth (Agip 1987), which are consistent with tomography velocities in the same depth range.

de Lorenzo et al. (2001) and De Siena et al. (2010) found evidence for an anomaly of low P-wave attenuation (low Qp) and high temperature between 2 and 3 km depth, occurring along the eastern onshore sector of the caldera rim. These observations led the authors to suggest that this anomalous zone could be the site where intense fracturing may have occurred during caldera collapse and resurgence, thus representing a preferential pathway for magma to migrate toward the surface and then erupt. This hypothesis is also supported by the presence of eruption

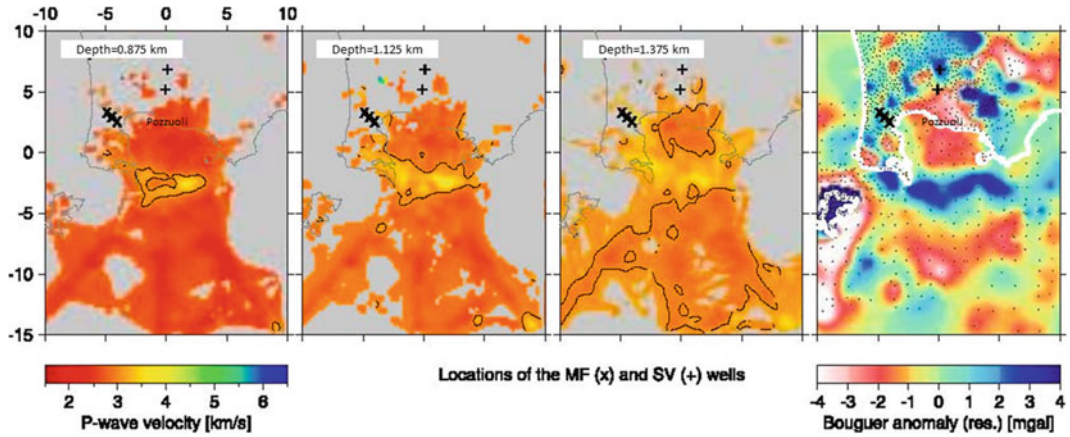

Fig. 7 P-wave velocity and Bouguer gravity anomaly images. The tomography P-wave velocity images are displayed from the left to the right at three different depths (875, 1,125 and 1,375 m). Symbols "+" and "×" indicate the location of S. Vito and Mofete wells, respectively, drilled by AGIP in the late 1970s for geothermal exploration purposes. A low-pass filtered map of the Bouguer gravity anomaly (reduction density: 2.4 g/cm^3) is shown on the rightmost panel (after Zollo et al. 2003)

vents along or nearby the onshore sector of the eastern caldera rim.

Consistently with seismic results, the density model locates below 600 m depth the top of the caldera rim, marking a density discontinuity. The caldera top is not flat, but deepens from north to south of about 800 m. The caldera low density has a diameter of ~6 km, even if it is characterised by a complex structural pattern of blocks that have undergone differential movements, are located at different depths and are separated by structural lineaments (Fig. 5). In fact, the 3D density anomalies distribution sketches a pseudo-circular high-density feature, encompassing an inhomogeneous low-density crustal sector. The pseudo-circular feature shows a complexity in its south-eastern portion, likely related to activation in that area of portions of northwest-southeast trending regional faults during the CI and NYT collapses (Capuano et al. 2013; Chap. Volcanic and Deformation History of the Campi Flegrei Volcanic Field, Italy).

The complex arc-shaped velocity anomaly has a close counterpart in the density model. In fact, a high-density pseudo-circular feature encloses the caldera both inland and offshore (Fig. 8). The continuity of this feature is well established except in the north-eastern sector of the caldera, where it is less marked and interrupted by structural discontinuities. In this part of the caldera, the high-density margin may be partly obliterated by the post-caldera volcanism that concentrated in this sector. A few small discrete density highs located at shallow depth (about 1 km) may be recognised along this feature, one of these being closely correlated with the Monte Gauro volcano and another, with very small lateral dimension and more similar to a conduit, being closely correlated with Astroni. These anomalies may be related to the remnant of the feeding system of the post-NYT eruptions.

The portion encompassed by the pseudo-circular high-density feature can be subdivided into a north-eastern and a south-western sector, according to the complex distribution of anomalies. This subdivision is corroborated by the trending of morphostructural lineaments. The root of this pseudo-circular anomalies' alignment appears to extend down to about 2,500 m. In fact, at 3 km depth the density contrast abruptly decreases and fades, likely in correspondence of the bottom of the caldera fill, consistently with the seismic results. The density distribution, the caldera structural boundary and the post-collapse deformation pattern support piecemeal collapse and block resurgence mechanisms (Capuano et al. 2013; Chap. Volcanic and Deformation History of the Campi Flegrei Volcanic Field, Italy).

Down to 4–5 km depth beneath the CFc, no evidence is found in the current 3D P-wave velocity images for magma bodies with volumes greater than 1 km^3. This would imply that the main magma reservoir feeding the Phlegraean magmatic system has to be located deeper, well within the carbonate basement. On the other hand, the results of the attenuation tomography study by De Siena et al. (2010) using local earthquake data have suggested the presence of small batches of molten rocks in the same depth range, based on the interpretation of low-velocity, high attenuation anomalies. However, since the resolution of the tomography method degrades with the size of such an anomaly, it is likely that 1 km is the lower limit of its spatial resolution to reconstruct subsurface seismic images in this area with the current data (e.g., Battaglia et al. 2008). Future higher-resolution observing systems (i.e., dense 2D or 3D arrays of seismic antennas) likely will be able to clarify this important but still unresolved issue.

Re-interpretation and modelling of local earthquake data of the 1982–1984 bradyseismic crisis, recorded by the University of Wisconsin mobile network, also provided seismic images of the shallow caldera structure (Vanorio et al. 2005; Chiarabba and Moretti 2006; Battaglia et al. 2008). With the aim of exploring the structure of the caldera and the role of hydrothermal fluids on velocity changes, Vanorio et al. (2005) adopted a multidisciplinary approach based on three-dimensional delay time tomography and rock physics characterisation. Selected arrival time data were modelled using a three-dimensional tomography method, based on an accurate finite difference travel-time

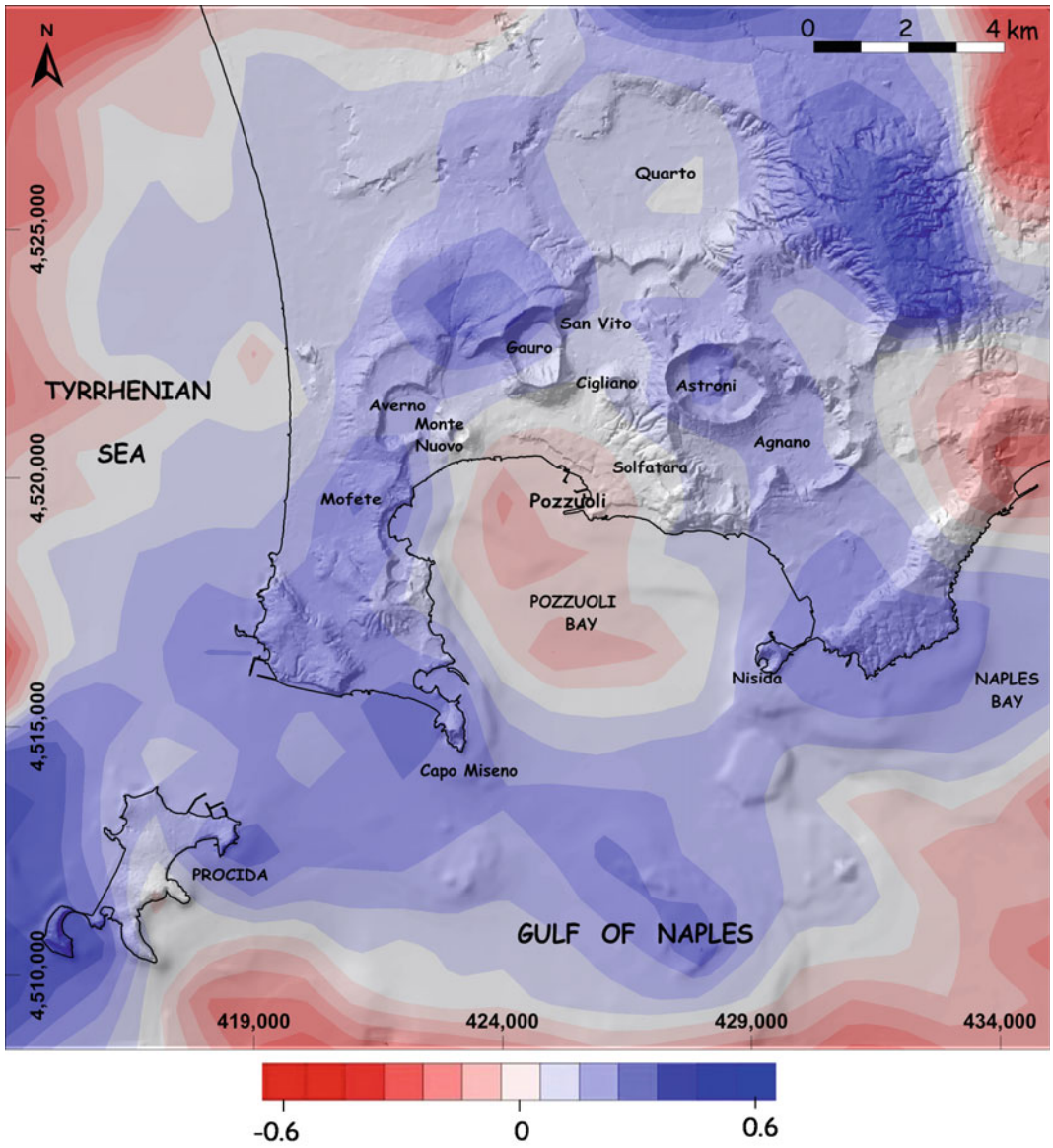

Fig. 8 Density horizontal slice between 2,200 and 2,600 m b.s.l. Colour scale represents density contrasts (g/cm^3). Figure modified after Capuano et al. (2013)

computation and a simultaneous inversion of P-wave and S-wave first-arrival times for both velocity model parameters and hypocentre locations (Latorre et al. 2004). Vanorio et al. (2005) interpreted the retrieved P-wave and S-wave velocity images as well as the deduced V_P/V_S images using experimental measurements of rock physical properties on Phlegraean samples to take into account steam-water phase transition mechanisms affecting the P-wave and S-wave velocities. Moreover, they constrained the role of over-pressurised fluids on velocity through modelling the petrophysical properties of site-relevant rocks. The authors located a flat and low V_P/V_S anomaly at 4 km depth under the town of Pozzuoli, below most of the events (Fig. 9). They suggested that this anomaly implies the occurrence of fractured, over-pressured gas-

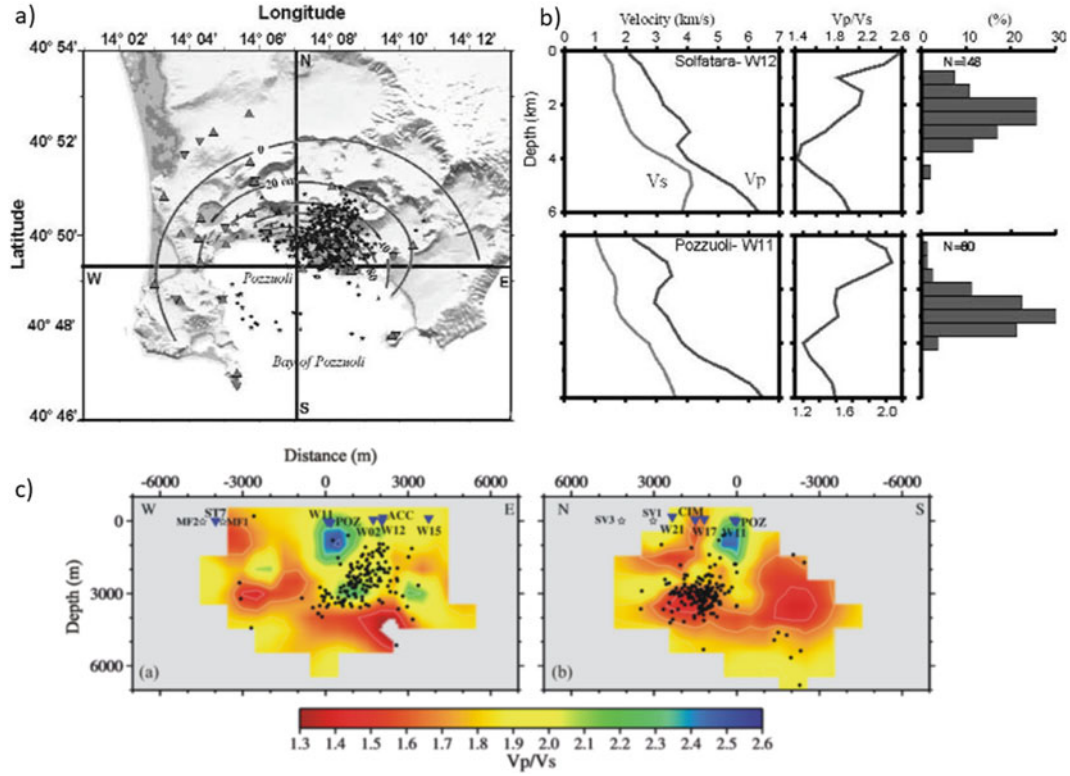

Fig. 9 **a** Map of the Campi Flegrei caldera showing seismometer stations (triangles) and final earthquake locations (stars) obtained by tomography inversion (from Vanorio et al. 2005). The map also reports the elevation contours (black lines) for the 1982–1984 uplift. **b** Reversal trends on vertical velocity profiles, V_P/V_S and histograms showing the earthquake distribution along profiles (radius equal to 0.5 km). **c** Vertical cross-sections of the variation of the V_P/V_S ratio and earthquake distribution (black points) along the east–west and north–south directions reported in **a**). Stars and triangles indicate wells and stations, respectively

bearing rock sequences and excludes the presence of molten rocks. Furthermore, they interpreted a high V_P/V_S anomaly found at 1 km depth as an evidence of the presence of rocks containing fluids in the liquid phase.

Battaglia et al. (2008) proposed a strategy for merging both active and passive datasets in a linearised tomography inversion and applied it to the whole active and passive Campi Flegrei datasets. This study provides the most comprehensive, integrated and best-constrained image reconstruction of the P-wave and S-wave velocity distribution beneath the caldera down to an approximate depth of 4–5 km. The P- and S-velocity models of the caldera structure were obtained by a tomography inversion based on travel-times recorded during two distinct experiments, the passive seismic data of the 1982–1984 crisis and the SERAPIS active seismic survey. Furthermore, their tomography inversion utilised an improved method based on an accurate finite-difference travel-time computation and a simultaneous inversion of both velocity models and earthquake locations.

The obtained images confirm the presence of a ring-like high P velocity in the southern part of the Pozzuoli Bay and extends its trace further inland as compared to previous results (Fig. 10). The V_P/V_S model confirms the presence of two characteristic features. A very high V_P/V_S anomaly at about 1 km depth below the town of Pozzuoli and interpreted as due to the presence of rocks containing fluids in the liquid phase. A low V_P/V_S body at about 3–4 km depth below a large

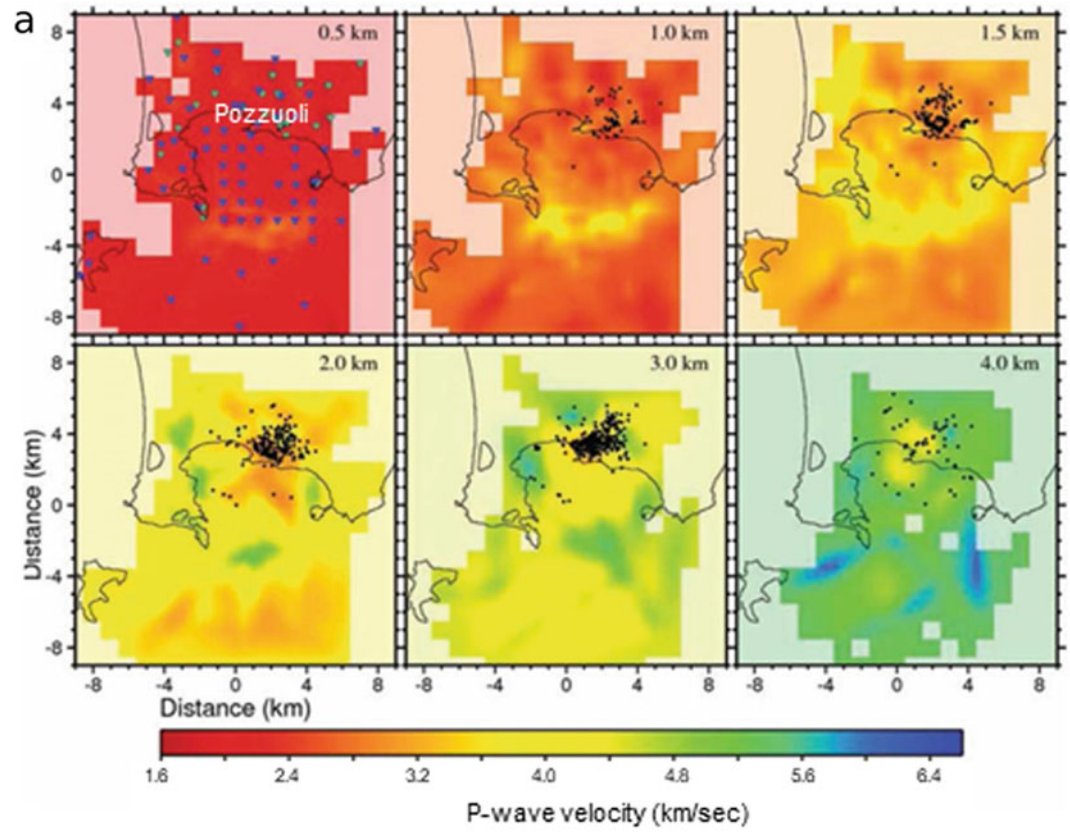

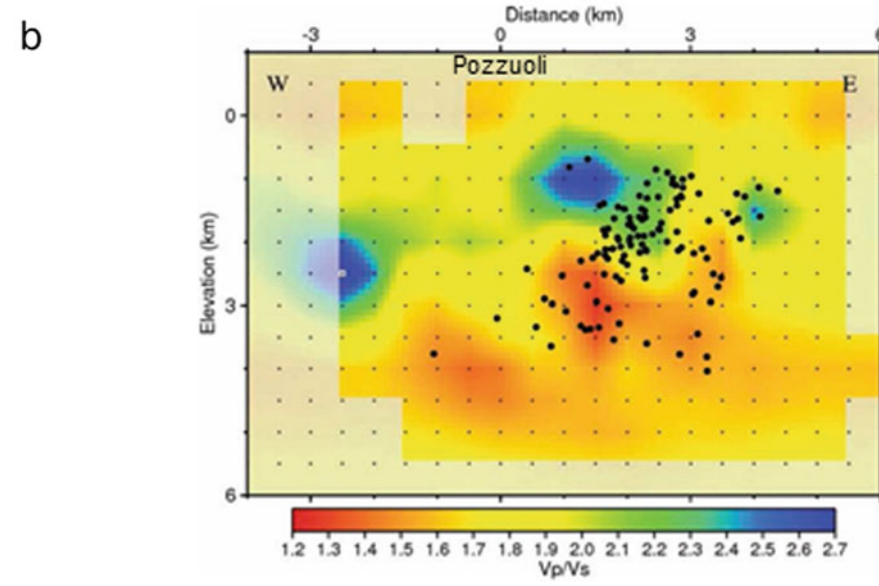

Fig. 10 Tomography results for Campi Flegrei obtained by inversion of active and passive data sets. **a** Horizontal sections of the P-wave velocity model at different depths (showed in each panel). **b** East–west cross-section at y = 2.5 km of the V_P/V_S ratio. Figure modified after Battaglia et al. (2008)

part of the caldera is interpreted as the top of rock bodies enriched in gas under supercritical conditions, as previously suggested by Vanorio et al. (2005).

As discussed by Vanorio et al. (2005), fluid overpressure that can result from fluid expansion, among other factors, can, in turn, cause the reversals in both P-wave and S-wave velocity logs, as it prevents the effective stress from increasing as fast as it would under normal hydrostatic or lithostatic pressure conditions. The P-wave velocity logs from the −1 to −3 km depth boreholes indicate a reversal stronger than that of the S-wave velocity, which is ultimately responsible for the observed decrease in the V_P/V_S value (cfr. Fig. 9). This would imply that P-wave velocity reversals are further enhanced by the presence of gas in addition to dense fracturing. Fracturing, under the hypothesis of overpressure, affects both P-wave and S-wave velocities while earthquakes mainly occur both at the top of reversal trends and within the low V_P/V_S zone. This evidence supports the hypothesis that the low V_P/V_S anomaly occurring at 4 km depth beneath the centre of the caldera and below the reversal velocity zone is due to the presence of over-pressured gas-bearing rocks at supercritical conditions (temperatures of about 400 °C were reported in the San Vito well at 3 km depth (Agip 1987).

3.3 Mesozoic Carbonate Bedrock, Including Magma Layers (from ~4 to ~12 km Depth)

3.3.1 The Top of the Mesozoic Carbonate Sequence

Judenherc and Zollo (2004) processed the Serapis P-wave travel-time collection, extended with a previously acquired dataset from the TomoVes experiment at Somma-Vesuvio, and computed the most comprehensive 3D P-wave velocity model for the Gulf of Naples and a small-scale high-resolution model for the CFc. The joint interpretation of the velocity distribution together with the available gravity data and the geothermal drilling information (Agip 1987) permitted to identify and map lithological units at depth. In particular, the tomography images and the apparent velocity (V_P ~6 km/s) of secondary head wave arrivals on seismograms indicate the existence of the Mesozoic carbonate sequence at about 4 km depth beneath the caldera (Fig. 11). This discontinuity is a continuous structural feature well detected in 3D tomography images and marks the sharp P-wave velocity increase from 3–4 to 5–6 km/s between 2 and 4–5 km depth in the shallow crust beneath the Naples and Pozzuoli bays. These results corroborate the observations from previous seismic reflection soundings in the area (e.g., Finetti and Morelli 1974).

At the wider regional scale, the Judenherc and Zollo (2004) velocity model reveals two main fault steps that affect the Mesozoic carbonate sequence (Fig. 11). Both tectonic features are interpreted as normal fault systems that deformed the Mesozoic carbonate sequence during the middle Pleistocene northwest-southeast extension. The south-eastern step corresponds to a southwest-northeast trending normal fault system (Finetti and Morelli 1974; Bonasia et al. 1985) that likely reaches Somma-Vesuvio toward the northeast (Bruno et al. 1998). The model also indicates a vertical offset of about 1,000 m, which affects the 1–2 km and 2–3 km layers. This offset is compatible with the interpretation of reflection data, indicating a rapid deepening of the top of the carbonate sequence from less than 1,000 m b.s.l. off the Sorrento Peninsula to more than 2,500 m b.s.l. in the central portion of the Gulf of Naples (Finetti and Morelli 1974). The north-western step is parallel to the south-eastern one and runs from the eastern rim of the caldera toward the southwest, along the 35-km-long segment of the Posillipo—Banco di Fuori fault system (Judenherc and Zollo 2004). The vertical slip along this fault system is similar to that along the south-eastern one, which affects the 3–4 km and 4–5 km layers (see Fig. 11). The height of the scarp is thus between 1,000 and 2,000 m.

The evidence for a geometric relation between the location of the CFc and the north-western normal fault affecting the carbonate sequence led Judenherc and Zollo (2004) to suggest that the deep magmatic feeding system of the Campi

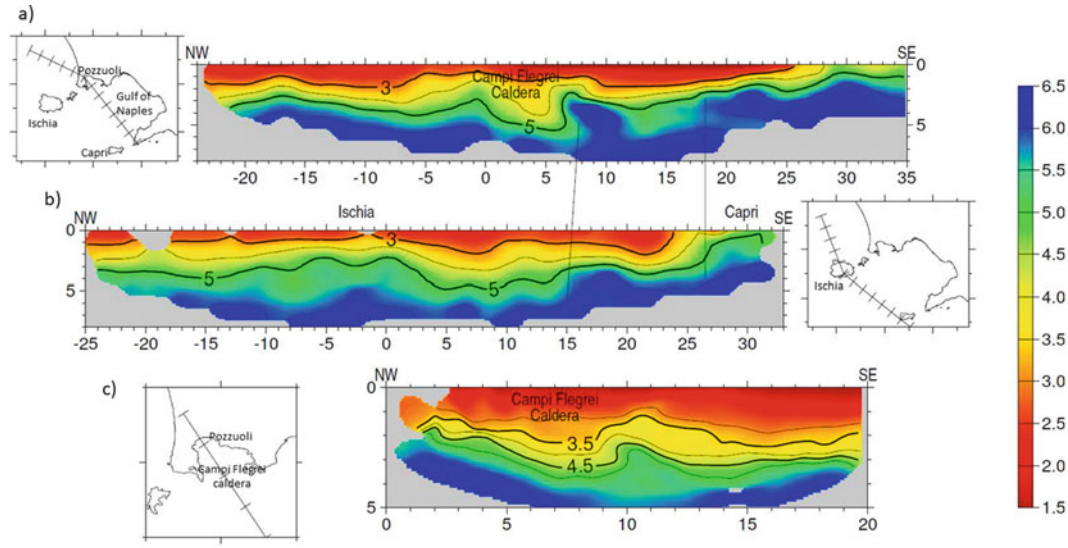

Fig. 11 Selected cross sections in the Gulf of Naples (top and centre) and Bay of Pozzuoli (bottom) tomography models (no vertical exaggeration). The inset maps show the traces of the cross sections, and the tick marks are at 5 km spacing. The two cross sections in the Gulf of Naples clearly show the normal faults affecting the carbonate sequence; their locations are indicated by the thick lines (from Judenherc and Zollo 2004)

Flegrei volcanoes could be related to this fault system, as the caldera structure lies just above it. Therefore, the normal fault system affecting the carbonate sequence could provide a preferential pathway to molten material located in a deeper magma reservoir, embedded within or beneath the carbonate sequence, for ascent. They also indicate that a similar geometric relation between Somma-Vesuvio and an analogous normal fault with the same orientation exists and suggest that this fault controls the magma displacement toward the surface in an equivalent way to the similarly-trending fault system beneath the CFc (Moretti et al. 2013 and references therein).

3.3.2 Main Crustal Discontinuities Beneath the Caldera from Seismic Reflection Analysis

The tomography velocity models from first-arrivals derived for the CFc reach a maximum depth of about 5–6 km. For a greater depth penetration of rays, either larger source-receiver distances or (earthquake) sources at greater depth would be required, or secondary waves such as reflections and conversions can be used. With the aim of characterising also the deeper structure beneath the CFc, Zollo et al. (2008) analysed reflected and converted wave amplitudes from main seismic horizons in a large subset of the SERAPIS data available within the caldera. The seismic reflection amplitudes depend on the impedance (product of velocity and density) contrast at the reflectors and the ray incidence angles or the source-receiver offset, thereby providing information on the velocities in a layer below the reflector. To include both P-wave and S-wave information and to remove unwanted source and receiver site effects, Zollo et al. (2008) analysed the ratio of the PP to the PS converted phase from the same reflector. Details of the method as well as its advantages and limitations are described in Maercklin and Zollo (2009).

About 75,000 three-component records acquired at 30 sea-bottom stations have been initially arranged in Common Midpoint gathers with 500 × 500 m cell size and more than 120 records per gather in the centre of the Pozzuoli Bay. Data pre-processing included a 5–15 Hz band-pass and additional trace normalisation for phase identification. PP reflection and PS

conversion move-out analyses were applied using an average 1D velocity model derived from the 3D tomography models, and reflection events were identified based on lateral waveform coherency, move-out alignments and stack amplitudes of both vertical and horizontal component sections. The PP and PS amplitudes at the same interface were extracted from the seismograms at several source-receiver offsets, covering a distance range that was large enough for a significant PS-to-PP amplitude ratio variation with offset. The P-wave velocity and the V_P/V_S value above the reflecting interface were constrained by the travel-times, and the theoretical PS-to-PP amplitude ratios were computed using dynamic ray modelling, including the correction for geometrical divergence and assuming a constant rock density. The unconstrained model parameters V_P and V_P/V_S below the reflector were then varied to minimise the misfit between the observed and the theoretical ratios, and the best-fit model was found by inversion (Zollo et al. 2008; Maercklin and Zollo 2009). The final 1D average model was constructed in a layer-stripping procedure, starting with the shallowest reflector and moving subsequently downward.

Zollo et al. (2008) found three major reflectors around 0.6, 2.7, and 7.5 km depth, respectively (Fig. 12). The shallowest reflector corresponds to the base of the marine unconsolidated sediments discussed above. The 2.7-km-deep reflector is characterised by a well-constrained positive P-wave velocity contrast and a small value of V_P/V_S value below the reflector. Zollo et al. (2008), following a previous interpretation and rock physics modelling by Vanorio et al. (2005), attributed this reflector to the top of a supercritical fluid- or gas-bearing, thermo-metamorphic rock layer. The type of fluid or gas (i.e., CO_2 or vapour) could not be inferred from this seismic study because their physical properties at the high in-situ temperatures (up to 400 °C) are very similar and do not affect seismic velocities significantly. The thickness of the thermo-metamorphic layer also remains unclear, and the top of the Mesozoic carbonate sequence could not be identified as a contiguous reflector. However, the tomography P-velocities of 6 km/s (Judenherc and Zollo 2004) and some P-wave reflection energy imaged by Blacic et al. (2009) suggests the transition to the carbonate sequence at about 4 km depth beneath the CFc.

The 7.5-km-deep reflector shows a strong negative velocity contrast with a wide range of possible values for V_P and V_P/V_S below the reflector. An additional modelling of the relative P-wave amplitudes of the 2.7-km- and the 7.5-km-deep reflectors constrained V_P in the layer below the deepest reflector to about 2.8 km/s, which means a strong negative V_P contrast with an estimated V_P/V_S increase from 1.65 to 2.35 or even higher. According to Zollo et al. (2008) these values indicate that the 7.5-km-deep reflector corresponds to the top of a low velocity layer, whose seismic velocities are consistent with the values expected for a magma body set in a densely fractured volume of rock (Fig. 13). Under the simplifying assumption of a constant velocity within this layer, later reflections detected at some locations suggested that this layer is about 1.5 km thick. This led to the conclusion of an extended magma sill beneath CFc similar to the one found beneath the neighbouring Somma-Vesuvio (Auger et al. 2001).

Taking the P-wave reflection time picks of Zollo et al. (2008) for the three reflectors, Vassallo et al. (2010) made a first attempt to obtain a 3D model of the morphology of each reflector using a tomography inversion scheme (Hobro et al. 2003). The model is parameterised as a stack of layers separated by interfaces. The inversion process starts with a highly-smoothed model whose complexity increases at each step by adding smaller wavelengths until a satisfactory fit to the data is obtained. Using an optimised 1D P-velocity model as a starting model, the 3D morphology of each reflector beneath the caldera was seismically imaged separately, following a layer-stripping procedure beginning with the shallowest reflector. Figure 14 shows the obtained interface models along with their associated uncertainties. The 0.6-km-deep reflector indicate the approximate thickness of the very shallow and most recent layer composed of water-saturated volcanic deposits. The

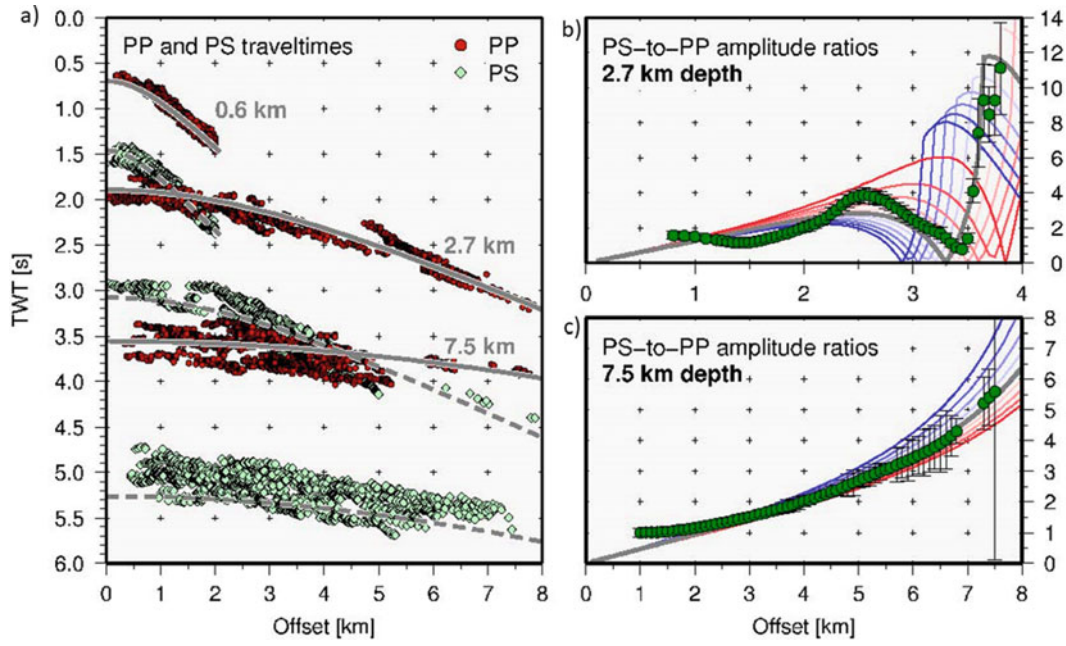

Fig. 12 Reflection travel-time curves. **a** P-to-P and P-to-S travel-time picks (dots) for three major reflectors overlaid with the theoretical times (grey lines) from a 1D average model. Average of the amplitude ratio variations with offset for reflectors at **b** 2700 m and **c** 7500 m depth. The figure shows the observed amplitude ratio (green dots), as compared with a set of theoretical curves computed for the V_P and V_P/V_S velocity contrast models. Given the best-fit model parameters at each interface, the blue and red curves indicate 10% positive and negative model variation with respect to V_P. Error bars for the estimated amplitude ratios are also shown. Density contrasts at both interfaces have not been included in the analysis, as this parameter has a minor effect on the amplitude ratio variation with offset (from Zollo et al. 2008)

2.7-km-deep reflector shows a well-resolved morphological high coinciding with the buried, southern caldera rim and a basin-like structure toward its central portion. The 7.5-km-deep reflector appears essentially flat, being characterised by variations smaller than the estimated depth uncertainty with a minor up-doming feature toward the southwest.

3.3.3 A Magma Sill Beneath the Caldera

The interpretation of the seismic low-velocity layer below the 7.5-km-deep reflector as an extended magma sill (Auger et al. 2001; Zollo et al. 2008) is supported also by petrological data (Mangiacapra et al. 2008; Pappalardo and Mastrolorenzo 2012a, b; Moretti et al. 2013). It should be noted that Ferrucci et al. (1992) previously found evidence for a magmatic body between 4 and 6 km depth beneath the caldera. These authors based their claim on direct P-wave and converted-transmitted PS-waves from a single 1-ton explosion at sea, recorded in a fan-layout onshore at 60–65 km distance. In particular, they analysed the delay time between direct and converted wave and modelled the amplitude ratio between the two phases, indicating a low-rigidity (low-velocity) body.

Considering extrapolations of the average geothermal gradients below the critical point of water (at ~3 km depth), where the thermal regime is due to pure conduction, the temperatures in the layer below 7.5 km should be in the range of 800–1,600 °C (e.g., Carlino and Somma 2009). This is in favour of the interpretation of seismic low velocities as due to the presence of melt instead of, for example, porous, brine-saturated rocks. The melt fraction in this layer

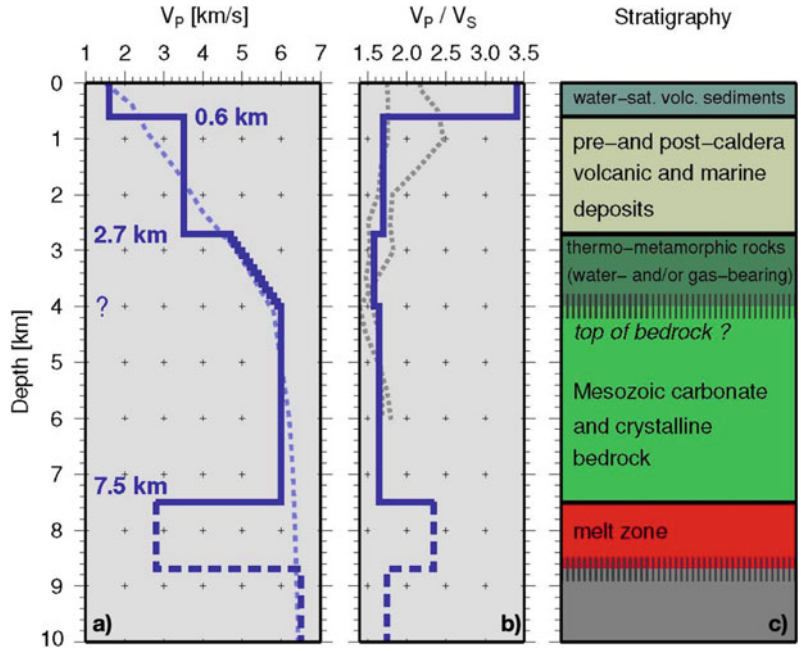

Fig. 13 Geophysical and structural model of the deep structure of the Campi Flegrei caldera. **a** Average 1D P-velocity model for the Campi Flegrei caldera, based on PP and PS travel-times, and on PS-to-PP amplitude ratios. The dashed line is the average of the 3D P-velocity model in the study area. **b** V_P/V_S ratio as a function of depth, as estimated in Zollo et al (2008). The dotted lines are two V_P/V_S depth profiles estimated from the local earthquake tomography (Vanorio et al. 2005). **c** Stratigraphic model. Figure modified after Zollo et al. (2008)

can be estimated using an appropriate rock physics model to relate the detected seismic velocities to the physical properties of a mixture of melt and solid. To get such an estimate, Zollo et al. (2008) computed Hashin–Shtrikman bounds (e.g., Mavko et al. 1998) on seismic P-wave and S-wave velocities for a two-phase medium consisting of solid rock and pure melt. The Hashin–Shtrikman bounds provide the narrowest possible range of the elastic moduli (or seismic velocities) by assuming an isotropic mixture of the two constituents without the need of specifying their geometry. Zollo et al. (2008), based on the results of laboratory measurements on similar rock types (Murase and McBirney 1973), used values of V_P = 5.5 km/s and V_S = 3.2 km/s for the solid phase, and of V_P = 2.4 km/s and V_S = 0 km/s for the pure melt, while the density was held constant at 2,600 kg/m^3. These boundary values indicate the presence of 65–75 vol% melt directly beneath the reflector, taking the obtained seismic velocities for the magma layer (V_P = 2.8 km/s and V_P/V_S = 2.35). However, it has been proposed that magmas at depth could crystallise in cooler regions generating non-zero Vs, which would lead to an even higher percentage of melt fraction (for details see discussion in Zollo et al. 2008). On the other hand, Chu et al. (2010) found a similar seismic velocity structure beneath the Yellowstone caldera from the analysis of teleseismic P-waves, but estimated a melt fraction of only 32 vol% (see also Fedi et al. 2018). Although initially developed for unconsolidated sediments, Chu et al. (2010) used a rock physics model based on the Gassmann relations for porous, fluid-saturated media and the concept of a critical melt fraction, at which the solid medium would break down and become suspended in the fluid (e.g., Mavko et al. 1998). Albeit these variations, seismic evidence shows clearly an extended sill containing a high melt fraction at mid-crustal depths beneath the CFc, and the presence of a similar feature at the same depth beneath Somma-Vesuvio could suggest a

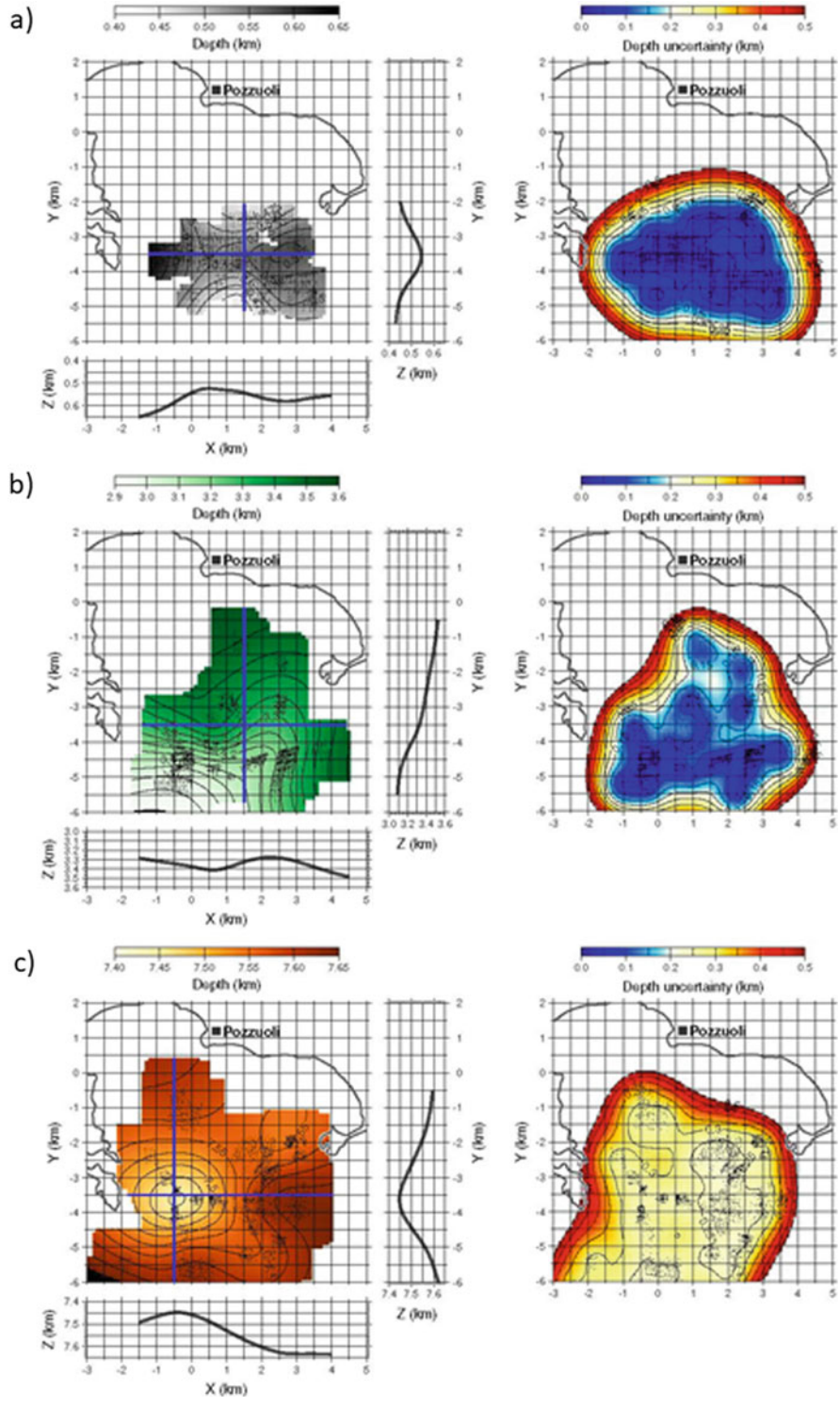

Fig. 14 Reflection interfaces obtained from the inversion of P-to-P travel-times associated with phases reflected from the first (**a**), second (**b**) and third (**c**) discontinuity. The left-side panels show the areal distribution of the reflectors and the vertical sections computed along the north–south and east–west oriented blue lines. The right-side panels show the computed uncertainties associated to the parameters of the models. The small black dots are the positions of the reflected impact points (from Vassallo et al. 2010)

common magma reservoir of these two volcanoes, as also proposed by Pappalardo and Mastrolorenzo (2012a, b). The existence of a shallow, extended and fractured rock layer saturated with supercritical fluids, above a mid-crustal melt zone, is also consistent with similar observations at other unrest calderas, such as Yellowstone, Socorro and Long Valley (DeNosaquo et al. 2009; Fialko et al. 2001).

3.4 Lower Crustal Structure and Moho (from ~12 to ~30 km Depth)

Rather little is known on the lower crust beneath the CFc from seismic data. In a regional crustal thickness model for Italy, Di Stefano et al. (2011) suggested that the Moho beneath the CFc and the Somma-Vesuvio is at 27 km using an interpolated value as in other regional Moho maps. Ferrucci et al. (1989) found a major Moho upheaval beneath the CFc, using data from two large-explosion-source locations at sea (3 × 1-ton and 2 × 0.5-ton) recorded inland in arc-shaped receiver spreads (fan-shooting geometry). The source-receiver distances ranged from ~ 45 to 100 km, covering both the CFc and Somma-Vesuvio. Ferrucci et al. (1989) developed an essentially 1D P-velocity model using detected reflection travel-times and amplitudes, and Gaussian-beam ray-tracing modelling. In their model the lower-crustal P-velocities show typical values for a continental lower-crust in which the P-velocity increases from 6.2 to 6.6 km/s between 12 and 18 km depth. This layer is underlain by a 7-km-thick high-velocity layer with a P-velocity of 7.2–7.3 km/s. Ferrucci et al. (1989) identified the Moho depth at 25 km beneath the CFc and at 35 km beneath the nearby Somma-Vesuvio. To date these are the only published images of the lower crust below the magmatic layer at 7.5 km depth based on the results of active seismic surveys. However, the structure of lower crust has been recently hypothesised through an interpretation of the large gravity low centred beneath the Gulf of Naples in terms of density distribution (Fedi et al. 2018). The modelling suggests large volumes of partially molten rock (~30 vol%) distributed randomly throughout the entire lower crust sector, likely made up of crystalline rocks largely produced by accumulation of crystals left by magma risen in the past.

In a complementary work, Nunziata and Costanzo (2010) derived average crustal S-wave velocity profiles from surface wave dispersion curves for a three travel paths between local earthquakes around Somma-Vesuvio and permanent seismic stations located within the CFc. To extract the fundamental Rayleigh wave mode, the authors applied a Frequency-Time Analysis to instrument-corrected radial-component seismograms, and then used data in the period range 1–5 s to invert for a 1D S-wave velocity model along each observation path. The typical lower-crustal S-velocity is ~3.6 km/s. Besides that, the models by Nunziata and Costanzo (2010) feature an S-wave velocity reduction at 7–15 km depth, again consistent with the presence of melt at these depths.

4 CFc Structure Deduced by Attenuation, Scattering and Ambient Noise Imaging

4.1 Direct-Wave Attenuation Images

Seismic attenuation tomography has been performed at the CFc using the waveform dataset from both the 1982–1984 unrest episode and the SERAPIS experiment. de Lorenzo et al. (2001) obtained the first 3D Q_P image of the CFc. Three-component waveform data from 87 micro-earthquakes recorded in March–April 1984 imaged Q_P in the shallowest 3 km of the central part of the caldera. The authors estimated the rise time and the total pulse width for direct P-waves, obtaining around 1,000 pulse data. These were inverted with a non-linear approach, retrieving attenuation images at a maximum resolution of ~1 km. Q_P models were transformed into temperatures by calibration with surface and borehole temperature data.

De Siena et al. (2010) expanded the dataset in time (January–June 1984) to 246 earthquakes

(location errors < 300 m). They used the coda-normalisation method (Aki 1980; Del Pezzo et al. 2006), removing source and site trade-offs by dividing direct energy. Coda energy is assumed constant in space. A ray-bending technique was carried out in the velocity model obtained by Battaglia et al. (2008). The work performed resolution tests, allowing for a theoretical maximum resolution of 0.5 km across the wider caldera, between 0 and 4 km depth. De Siena et al. (2010) applied their method jointly with the more standard spectral-decay method, which allowed a joint description of both Q_P and Q_S. The P- and S-waves attenuation features from De Siena et al. (2010) are compared with the V_P/V_S anomalies from Battaglia et al. (2008) in Fig. 15. Horizontal slices have been obtained at depths of 200, 1,200, 2,200 and 3,200 m b.s.l. and redrawn after space interpolation with the methodology described by Del Pezzo and Bianco (2013b). Due to the maximum resolution available, each image reflects the average attenuation structure in a layer with a thickness of 500 m, centred at the depth values indicated above. A dashed line borders the areas with the highest resolution in the attenuation tomography, and symbols (X1 through X7 in Fig. 16) mark the main volcanological features of the area under study, listed in the caption of Fig. 16. Serlenga et al. (2016) obtained the only attenuation tomography model for the offshore portion of the caldera in the Pozzuoli Bay and independent of the 1982–1984 unrest using data from the SERAPIS experiment. They use the spectral decay method in analogy to De Siena et al. (2010), detecting structures at a resolution higher than 1 km across the offshore portion of the caldera down to a maximum depth of 2 km.

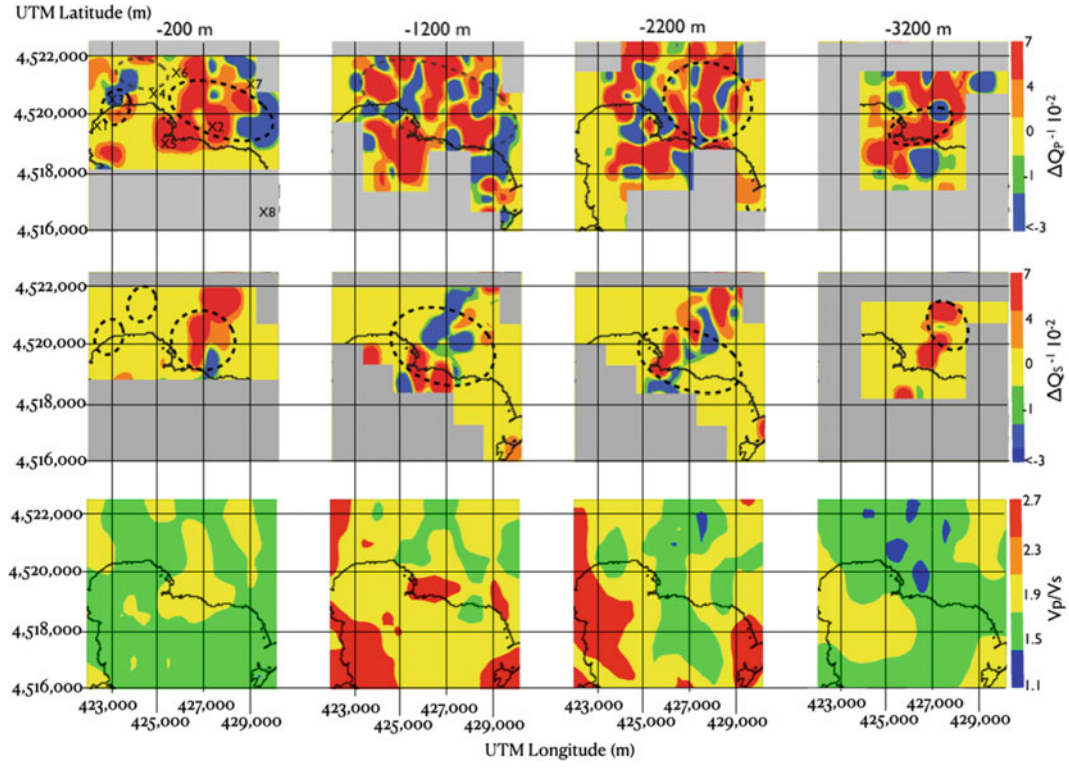

Fig. 15 Horizontal slices intersecting CFc at different depths showing variations of P-wave (top row) and S-wave (middle row) attenuation relative to the average quality factors. The V_P/V_S model (bottom row), redrawn after Battaglia et al. (2008), is compared with the attenuation models. The maximum resolution areas (500 m) are contoured with bold black dashed lines

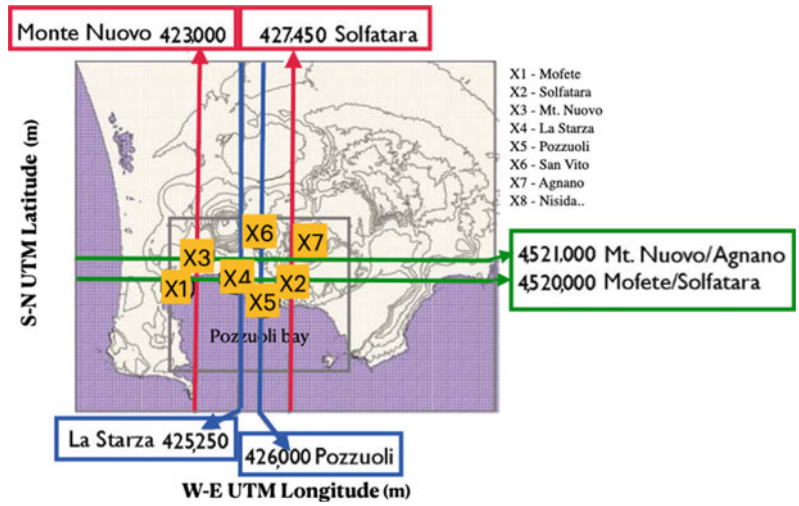

Fig. 16 Map of Campi Flegrei; the rectangle highlights the area investigated in De Siena et al. (2010). The lines define the spatial locations of the vertical sections associated with the tomography images of Figs. 17 and 18. The locations of the area of major volcanological interest are indicated as follows: X1 = Mofete, X2 = Solfatara, X3 = Monte Nuovo, X4 = La Starza, X5 = Pozzuoli, X6 = San Vito, X7 = Agnano

The upper 500 m at the CFc show small P-wave attenuation contrasts (see slice at -200 m in Fig. 15 and the vertical sections in Fig. 17). The Solfatara area (marker X2, Fig. 15 top left panel) in the maximum resolution volume (bordered by a dashed line) shows high attenuation. Moving from Solfatara toward the northeast, high-attenuation values extend to the Astroni - Agnano area (marker X7, northeast of Solfatara) as in de Lorenzo et al. (2001). Toward the northwest, the highest attenuation characterises the region of San Vito (marker X6). A lower-attenuation volume (yellow) separates Solfatara, Astroni and San Vito (markers X5–Pozzuoli and X4–La Starza zone) from high-attenuation rocks under Monte Nuovo and Mofete (marker X1 and X3). The position of this last zone agrees with the aquifer with temperatures between 100 and 130 °C recognised by Todesco et al. (2003) in the depth range 150–300 m b.s.l. The corresponding S-wave attenuation image shows lower attenuation in this depth range. At Solfatara, S-wave attenuation is high, similar to what found for the P-waves. Unlike P-waves, this zone is bordered east by a low attenuation anomaly, at the location of the high-velocity caldera rim (Battaglia et al. 2008).

The images in the three rightmost panels of Fig. 15 representing the space distribution of the attenuation anomalies, show a general laterally heterogeneous distribution pattern. Volumes characterised by rocks with high attenuation anomalies are interconnected with low attenuation zones. It is also noteworthy that high S-wave attenuation zones depict a vertically extended high attenuation pattern between about 3,500 m b.s.l. and the surface (Figs. 17 and 18). The images in Fig. 17 show strong lateral attenuation contrasts. High P- and S-wave attenuation volumes extend vertically between approximately 1,000 and 2,500 m b.s.l. under Mofete (Fig. 17, dashed rectangle #2) and Monte Nuovo (Fig. 17, dashed rectangle #1). The P-wave high attenuation volume under Solfatara extends from the surface down to 3,500 m b.s.l. (Fig. 17, dashed rectangle #6). Volumes of high attenuation match those with the V_P/V_S ratio only down to depths of 2 km. High-temperature fluids comprising carbon dioxide (Caliro et al. 2007) or supercritical fluids (Vanorio et al. 2005) developing under the CFc "caprock" could equally be responsible for these high attenuation volumes (Fig. 17, dashed rectangle #1). The high Q_S^{-1} volumes characterised under Mofete (X1) and Solfatara

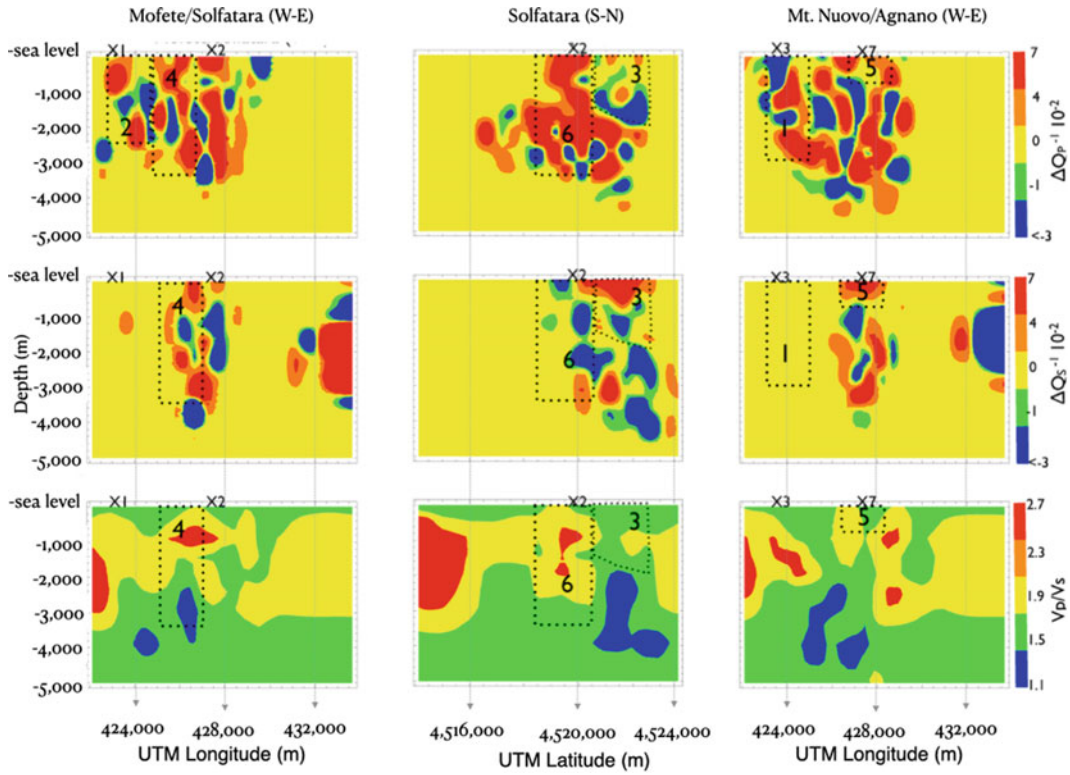

Fig. 17 Attenuation tomography results showing P-wave (top row) and S-wave (middle row) attenuation variations along three vertical sections passing through Mofete/Solfatara (east–west), Solfatara (north–south) and Monte Nuovo/Agnano (east–west). The last line shows V_P/V_S variations from Battaglia et al. (2008, redrawn). The columns are labelled with the name of the area crossed by the section and with the marker highlighting the area of volcanological interest (Fig. 16). The colour scale represents the variations from the average S- and P-wave inverse quality factor. The dashed numbered polygons contour the volumes discussed in the text

(X2) in Fig. 17 (dashed rectangle #4) coincide with the position of deep aquifers (1,250–1,600 m b.s.l.) recognised by Todesco et al. (2003). Under Agnano (Fig. 17, marker X7), high $Q_P^{-1}$and Q_S^{-1} in the shallowest kilometres of the crust coincide with a zone of moderate ($\geq$ 1.9) V_P/V_S anomaly (Fig. 17, dashed rectangle #5), where temperatures are on the order of 250 °C (de Lorenzo et al. 2001; Todesco et al. 2003). North of the Solfatara (X2), a very-low Q_P^{-1} anomaly characterises volumes down to the depth of 2,500 m b.s.l. (Fig. 17, dashed polygon #3). V_P/V_S shows a relative minimum in this area, while Q_S^{-1} is generally high (Fig. 17, dashed polygon #3). As high-temperature rocks (de Lorenzo et al. 2001), conductive heat transfer (Todesco et al. 2003), and low V_P (Battaglia et al. 2008) characterise this region at shallow depths (Fig. 17, dashed rectangle #5), De Siena et al. (2010) inferred the presence of a small reservoir of gas (mainly CO_2) feeding fumaroles (Caliro et al. 2007). The results confirm that fumaroles are the consequence of fluid migration from a magmatic to a geothermal reservoir and from there to the surface, favouring a magmatic interpretation of the 1982–1984 unrest (Todesco et al. 2003; Caliro et al. 2007; Amoruso et al. 2008; Berrino et al. 2008; Moretti et al. 2013, 2020). The observation of very-low Q_S^{-1} contrasts with this interpretation (Fig. 17, dashed rectangle #6); however, the assumption used by the coda-normalisation method suffers in the presence of sharp horizontal interfaces, where coda waves get trapped or reverberate at low

frequency. This feature was interpreted by De Siena et al. (2010) as due to alternating heterogeneous layers that affected the coda wavefield, destabilising coda-normalised measurements. In the next section, we will discuss how this interface (seismic horizon) at a depth of 2 km has been resolved and included in direct-attenuation forward modelling (De Siena et al. 2017b).

A subvertical attenuation contrast images the high-angle "La Starza" fault (Di Vito et al. 1999—Fig. 18, dashed rectangle #7), which apparently extends down to at least 2 km depth. The area of the last eruption (Monte Nuovo, marker X3 in Fig. 15) is relatively homogeneous for both S-wave and V_P/V_S (Fig. 17). The high P-wave attenuation anomaly located under Pozzuoli, between 0 and 2 km depth, correlates with the high V_P/V_S value (V_P/V_S = 2.6) down to 2 km (Fig. 18, dashed rectangle #8). In the same volume, high Q_S^{-1} corresponds to the location of high V_P/V_S. The anomaly appears as an inclusion inside very-low attenuation volumes, supporting the existence of a hydrothermal reservoir under the city of Pozzuoli (Vanorio et al. 2005). The low-attenuation structure underlying the reservoir is the attenuation response of the seismic horizon, later interpreted as a "caprock" rich in hot hydrothermal fluids. One of the most prominent and debated results of De Siena et al. (2010) is the high Q_S^{-1} anomaly located between of 2 and 3 km depth under Pozzuoli (Fig. 17, dashed rectangle #4, between X1 and X2) that extends under Solfatara (Fig. 17, dashed rectangle #6). Under Pozzuoli, this anomaly corresponds precisely to the location of a high-gravity anomaly interpreted as a melt batch (Amoruso et al. 2008), whose degassing has been central for the development of the 1982–1984 unrest episode (Caliro et al. 2007). However, its lateral extension is at the limit of the method's

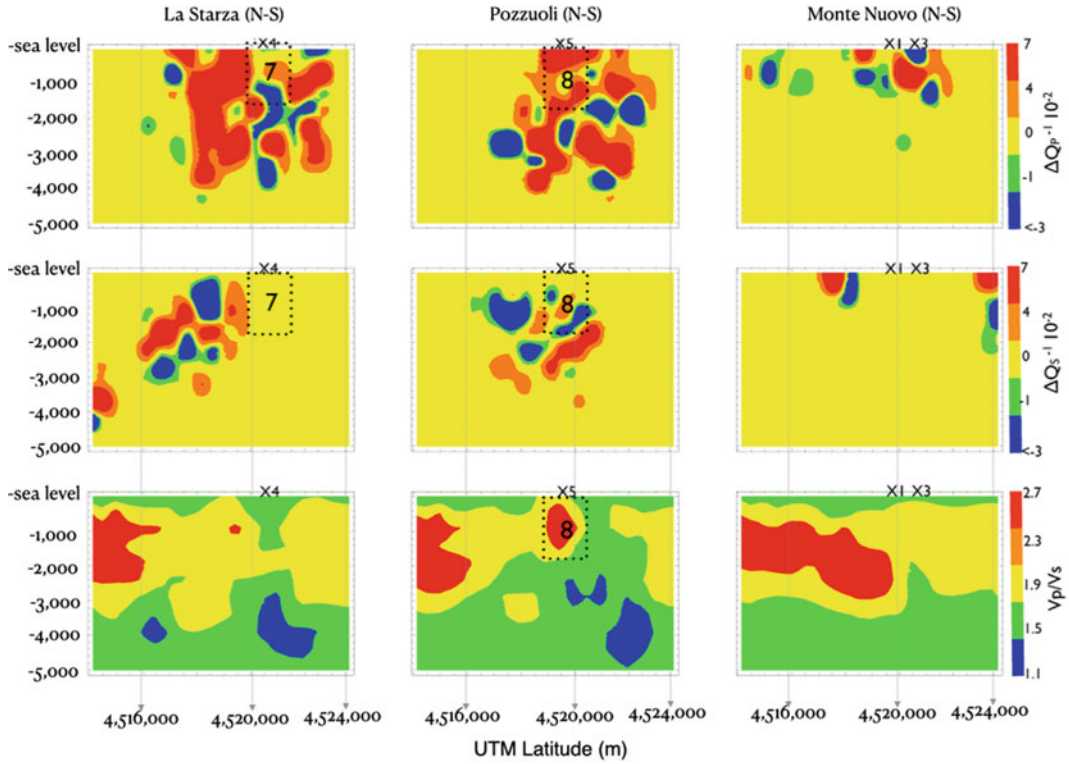

Fig. 18 Same as Fig. 17 for three vertical sections crossing La Starza (north–south), Pozzuoli (north–south) and Monte Nuovo (north–south). See Fig. 16 for section locations and labels

resolution at these depths. It also contrasts with the interpretations based only on the velocity images, as V_P/V_S value remains low under Pozzuoli and Solfatara (Vanorio et al. 2005). This trade-off has been tackled by following direct and coda-dependent methods applied to the same dataset, which remove faulty approximations from scattering dependent techniques (De Siena et al. 2017a, b; Akande et al. 2019) and use novel seismic tomography results at the caldera (Calò and Tramelli 2018).

The V_P/V_S model of Battaglia et al. (2008) shows two characteristic features across the offshore caldera. At about 1 km depth, a very high V_P/V_S anomaly occurs offshore the town of Pozzuoli and is interpreted as due to the presence of rocks that contain fluids in the liquid phase. A low V_P/V_S body extending at about 3–4 km depth below a large part of the caldera is interpreted as the top of rock bodies enriched in gas under supercritical conditions, as previously suggested by Vanorio et al. (2005). These fluids also produce high attenuation when they percolate in the shallower systems, either saturating sediments or remaining in a vapour phase. The strongest attenuation characterises the offshore caldera rim, which appears fluid-saturated in the uppermost 2 km of the crust (Serlenga et al. 2016).

4.2 Coda and Ambient Noise Imaging

Direct-wave attenuation combines both intrinsic and scattering effects: by separating these attenuation mechanisms and mapping them in space, we improve our ability to interpret structures. For example, low-velocity or high V_P/V_S anomalies corresponding to high attenuation can be interpreted as being due to the presence of: (1) a fluid or magma body, which would increase the shear-wave intrinsic attenuation with increasing temperature; (2) a partially saturated fracture network, which would produce an increase in scattering attenuation.

The joint interpretation of total attenuation and body-wave velocity tomography images suffers from this trade-off when locating and defining the extent of fluid reservoirs, magma batches, or the characteristics of a buried or submerged caldera rim. Scattering tomography detects sharp discontinuities in the elastic parameters (the position of the "strong scatterers"). It helps discriminate between zones with a high density of fractures (characteristic, e.g., of the caldera borders) and zones with large fluid reservoirs and magma intrusions (which can be associated with the active caldera centres). Scattering imaging has been applied to the CFc using different approaches (Tramelli et al. 2006; Maercklin 2008; De Siena et al. 2011, 2017a; Akande et al. 2019).

Tramelli et al. (2006) used a method developed by Nishigami (1991) that inverts the S-wave coda envelope fluctuations observed at a given lapse time in the coda of local earthquakes in terms of position and strength of the "strong" scatterers present in the Earth medium. The method computes seismic intensities at late lapse times in the coda and searches for the location and scattering coefficients that best fit it, with a search grid algorithm. The technique depends on the frequency-dependent transport mean free path and the assumption of diffusion. The equations of this method were originally written by Nishigami (1991) in the S-to-S single scattering assumption. Tramelli et al. (2009) demonstrated that this method is independent from the scattering model used to mathematically fit the average coda envelope, assuming that the coda envelope fluctuations are generated by S-to-S single scattering phenomena occurring at the "strong" scatterers. In Fig. 19, the stacks (over the components) of the values obtained from the inversion are showed separately for each frequency band. The inversion process returns the value of the scattering coefficient, $g = g_0\alpha_i$, in the i-th block. α takes into account the fluctuations of the scattering coefficient averaged over space (g_0). Figure 19 shows the space distributions of $\log(\alpha)$. The crosses and circles represent the scattering coefficients higher and lower than g_0, respectively. The results obtained in three layers spanning the shallowest 4 km of the upper crust show that the most heterogeneous materials correspond inland to the central portion of the

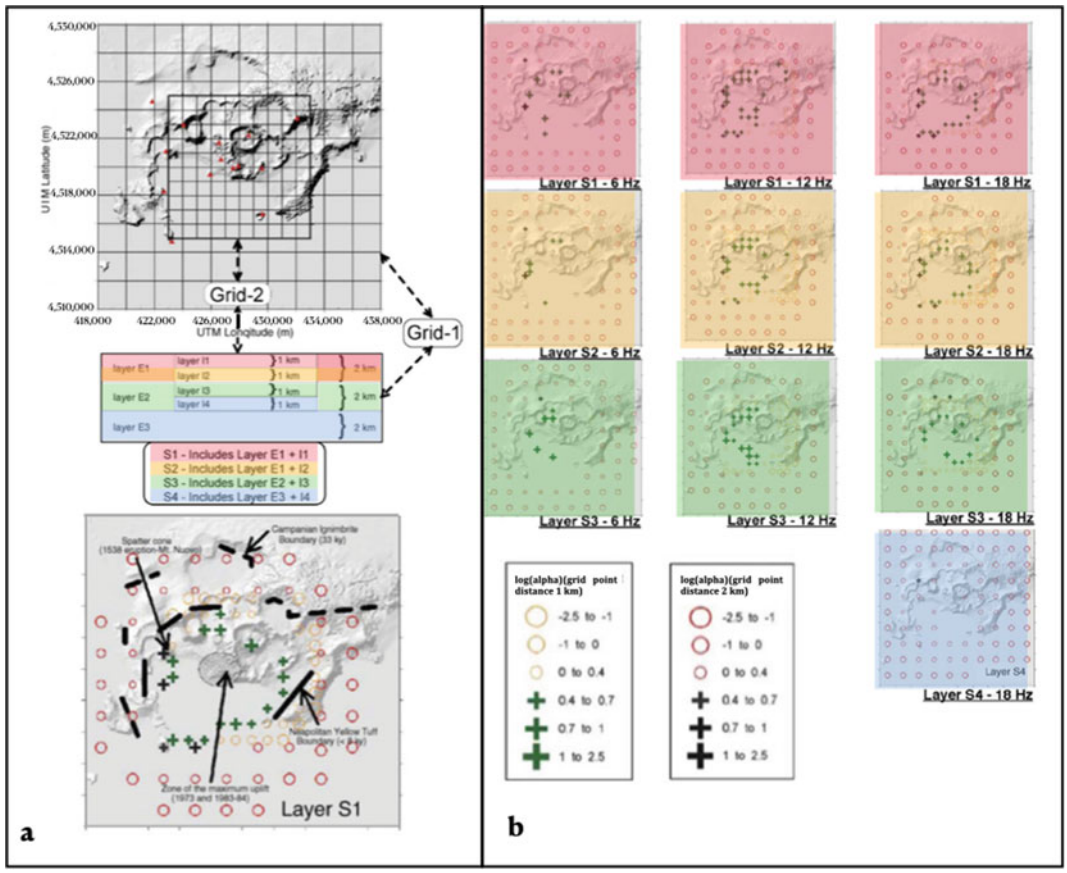

Fig. 19 Scattering image of the CFc: **a** at the top the scheme of the subdivisions with depth for the inversion, while the bottom part shows some geological features superimposed on the S1 layer at 18 Hz of panel b; **b** results of the inversions of the stacked (over the components) signals for several frequency. The crosses and the circles represent the areas with high and low scattering strengths, respectively as indicated in legend

caldera as mapped by velocity tomography. The authors deduced that similar anomalies in the submerged part of the caldera coincide with the submerged part of this structure. The assumption was confirmed by the offshore velocity tomography of Battaglia et al. (2008). The only high-scattering anomaly not directly connected to the rim appears in the eastern part of the caldera and corresponds to the high-temperature fractured body previously deduced by de Lorenzo et al. (2001) and later recognised by De Siena et al. (2010) from the contrasting P- and S-wave attenuation characteristics (Fig. 17, dashed rectangle #6).

Maercklin (2008) adopted an imaging method based on array beam-forming and coherence analysis of the P to P scattered phase, using the SERAPIS dataset. After grouping into arrays the signal sources, the author calculated the travel-times connecting any potential scatterer on a regular grid in the image volume to the source and receiver, using a 1D background velocity model. A high coherence measured on aligned traces indicates the presence of a scatterer at the corresponding location. A stack of the individual images from several pairs of a shot array and a single receiver provides the final image. Even in this approach, as in the previously described one,

the prominent region of seismic scattering roughly coincides with the high-gravity (Capuano et al. 2013) eastern buried caldera rim (Zollo et al. 2003). This work was the first to detect this volume in the offshore caldera.

De Siena et al. (2011) proposed a new quantitative approach for the joint interpretation of velocity and attenuation tomography images, which allows the separation of scattering and intrinsic attenuation. These authors used the P-wave tomography structure of Battaglia et al. (2008) to calculate the autocorrelation functions (ACF) of P-wave vertical velocity fluctuations from which the P-wave quality factor is estimated (see Eq. 6 in De Siena et al. 2011). A map showing the lateral variations of the ACF values (see Fig. 2 in De Siena et al. 2009) is then compared with the total-QP map (De Siena et al. 2010) using cluster analysis. The result is finally interpreted in terms of separation of intrinsic and scattering attenuation on a 2D plane. The resulting map (Fig. 20) shows:

1. a north–south scattering attenuation region located below the zone of the 1982–1984 maximum uplift, offshore the Pozzuoli Bay but also extending below Monte Nuovo. De Siena et al. (2011) based on the previous images in attenuation (De Siena et al. 2010), velocity (Battaglia et al. 2008) and S-to-S scattering (Tramelli et al. 2006), favour the interpretation in terms of a solid but fractured body, contoured by strong S-wave scatterers. They speculate that the high-scattering area corresponds to a section of the residual magma body associated with the AD 1538 Monte Nuovo eruption;
2. that the high-temperature volume originally detected by de Lorenzo et al. (2001) is the region where P-wave intrinsic dissipation dominates. The anomaly suggests a connection, valid for the uppermost 4 km of the crust, between the region offshore Pozzuoli and the Solfatara crater. The results agree with the existence of a paired Pozzuoli-Solfatara deformation source, active throughout the last 40 years (Amoruso et al. 2014).

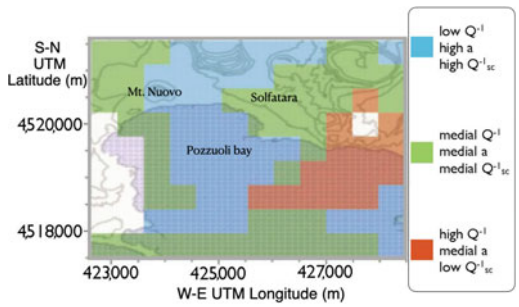

Fig. 20 Results obtained applying the cluster analysis to data from: total-Q^{-1}_P structure (De Siena et al. 2010), Q^{-1}_{Sc} measured by velocity fluctuations and correlation length, a (De Siena et al. 2011). This analysis shows the existence of three clusters (blue, green and orange). The physical characteristics of each cluster are indicated in the legend at the right side the of the map

During the last decade, researchers have developed a single open-access code that inverts for total, scattering and intrinsic attenuation from earthquakes and active seismic data simultaneously (MuRAT; De Siena et al. 2014a, b; Prudencio et al. 2015; Sketsiou et al. 2020). De Siena et al. (2017a, b) and Akande et al. (2019) applied this code to the 1982–1984 dataset. De Siena et al. (2017a) used 2D diffusive sensitivity kernels (Del Pezzo et al. 2016) to develop an inversion scheme for coda-wave attenuation (Qc) at multiple frequencies, allowing to model in space a quantity equivalent to absorption in the diffusive regime (Sketsiou et al. 2020). Akande et al. (2019) used 3D multiple-scattering kernels and the previous inversion scheme to obtain the 3D distribution of Qc in space. De Siena et al. (2017b) employed a revised coda-normalisation method that measures direct-wave attenuation, dropping the assumption of homogeneity of the coda wavefield. The authors interpreted the velocity and attenuation maps after re-localising the entire 1982–1984 earthquake dataset with a non-linear localisation approach (NonLinLoc; Lomax 2001). By pre-calculating source-station coda attenuation, they improved inversion residual by 80% relative to De Siena et al. (2010), removing ghosts in the outer caldera and obtaining maximum resolutions of 500 m in the eastern portion of the caldera. This work includes a time-dependent analysis of the 1982–1984

unrest through the joint description of seismic locations, attenuation and V_P/V_S anomalies.

The 3D P-wave velocity images described in previous sections find no evidence of magma bodies with volumes larger than 1 km^3 beneath the caldera. This would imply that the main magma reservoir feeding the Phlegraean magmatic system is deeper, within the carbonate sequence (Vanorio et al. 2005). The attenuation tomography study by De Siena et al. (2010) suggested the presence of low-velocities and high-attenuation batches of molten rocks (<1 km in size), correlated to high gravity anomalies at depths of ~3 km (Amoruso et al. 2008). However, the resolution of their tomography method degrades with the size of such an anomaly. One kilometre was the lower limit of spatial resolution to reconstruct subsurface seismic images in this area with the previously-mentioned techniques (e.g., Battaglia et al. 2008). More recently, Calò and Tramelli (2018) have reanalysed the 1982–1984 dataset using enhanced seismic tomography techniques, allowing theoretical resolutions of a few hundred metres. They found a high V_P/V_S anomaly between 2.3 and 4 km depth under the centre-eastern sector or the caldera, interpreting it as a plumbing system with a diameter of ~1 km. This is the first tomographic study to show prominent high V_P/V_S anomalies in this depth range and onshore. The model supports the presence of magmatic fluids or magma (Berrino et al. 2008; Amoruso et al. 2008) in the first 4 km of the crust in 1982–1984.

Calò and Tramelli (2018) also reconstructed a low V_P/V_S and high scattering anomaly (~500 m-thick) above the high V_P/V_S plumbing system. This is the same region where De Siena et al. (2010) had hypothesised the existence of a sequence of highly-scattering layers trapping coda intensities. De Siena et al. (2017b) imaged a low-attenuation seismic horizon under the entire caldera and particularly in this zone, compatible with the existence of the "caprock" recovered by rock-physics measurements at ~1–2 km depth under the caldera (Vanorio and Kanitpanyacharoen 2015). Under Pozzuoli and below this "caprock", De Siena et al. (2017b) imaged a low-velocity and high-attenuation anomaly, likely the response to deep fluids and magma. This anomaly, a reservoir of supercritical fluids (Vanorio et al. 2005) possibly intruded by small batches of magma (Amoruso et al. 2008) was the location of repeated seismic injections that opened the upper hydrothermal system in 1982–1984 (De Siena et al. 2017b). Once crossed with geochemical information, seismic tomography and source data confirm that this was also the primary location for processes causing geochemical and seismic unrest at the caldera in 1982–1984 (Chiodini et al. 2016, 2021). The seismic signature does not allow to discriminate dike intrusions from magmatic fluid injections but supports the existence of a magmatic component during the unrest (Amoruso et al. 2008; De Siena et al. 2010, 2017b; Moretti et al. 2020).

The deepest high-attenuation anomaly in De Siena et al. (2017b) plateaus at ~4 km depth and correlates laterally with the stationary deformation source active during the last four decades (Amoruso et al. 2014; Pepe et al. 2019). De Siena et al. (2017a) used the enhanced lateral resolution provided by the coda kernels to demonstrate that this high-attenuation structure produces a bulge in the low-attenuation caprock. This bulge corresponds to the source of deformation in the offshore central caldera, producing a single aseismic low coda attenuation anomaly (De Siena et al. 2017a). The ~4 km deep high-attenuation anomaly extends toward the eastern high-gravity sector of the caldera, connecting to the high V_P/V_S plumbing system (Calò and Tramelli 2018). Starting from de Lorenzo et al. (2001), all attenuation and scattering studies have found evidence of a fractured volume, producing high temperatures between 2 and 3 km depth across the eastern onshore sector of the caldera (see previous section).

Akande et al. (2019) used the 3D diffusive kernels to constrain the geometry of the connection between the deep source of the deformation and the Solfatara fumarole. They built a single interpretational model of the caldera using their coda-attenuation results, existing interdisciplinary knowledge, vents distribution (Orsi et al. 2004; Vilardo et al. 2010; Vitale and Isaia 2014; Chaps. Volcanic and Deformation History

of the Campi Flegrei Volcanic Field, Italy; Volcanic Hazard Assessment at the Campi Flegrei Caldera, Italy) and the novel V_P/V_S anomalies (Calò and Tramelli 2018). They confirmed previous inferences (de Lorenzo et al. 2001; Maercklin et al. 2008) by imaging a unique high-Qc^{-1} anomalous volume associated with the high-gravity region where intense fracturing occurs during caldera collapse and resurgence (Capuano et al. 2013). They additionally detected its connection to the primary deformation source in the central caldera. Figure 21 is a sketch that adds to their finding the results of velocity, attenuation, scattering and gravimetric analyses performed during the last four decades, showing them across an east–west profile passing through Pozzuoli. Akande et al. (2019) concluded that the high V_P/V_S, high Q_P^{-1} and Q_S^{-1}, high temperature, high-scattering and high-absorption capped pathway from deformation source to the eastern portion of the caldera represents preferential paths for magmas to intrude the crust in their ascent toward the surface and eventually feed eruptions. Recent seismic, gravity and electromagnetic investigations have focussed on the eastern sector of the caldera to resolve this issue (De Landro et al. 2017; Siniscalchi et al. 2019; Young et al. 2020), confirming the existence of a resistive plume structure in the uppermost 2 km of the crust (Siniscalchi et al. 2019).

The CFc has been mostly aseismic after its 1982–1984 unrest. The new unrest phase started at the end of 2004 and has been characterised by very low levels of seismicity until 2015 (Bellucci Sessa et al. 2021). Seismicity has recently increased, but ambient noise imaging has become the primary way to seismologically assess the caldera structure. De Siena et al. (2018) used phase-weighted stacking (Shimmel and Paulssen 1997) and the FMTOMO inversion framework (Rawlinson et al. 2004) to image surface group velocities between the surface and about 2 km depth. Pepe et al. (2019) used the ambient noise map to interpret the results of deformation gradiometry. These works suggest that the high V_P/V_S reservoir first detected by Vanorio et al. (2005) at $\sim$ 1 km depth (Fig. 21) has expanded north and west and become aseismic under the city of Pozzuoli. A seismic high-velocity structure north–south striking under Solfatara appears as a structural barrier for eastward deformation, in correspondence to the highly resistive plume (Siniscalchi et al. 2019). The analyses confirm the likelihood of an eastward-directed feeding system for fumaroles degassing at Solfatara and the new (2009) Pisciarelli vent (Chiodini et al. 2021).

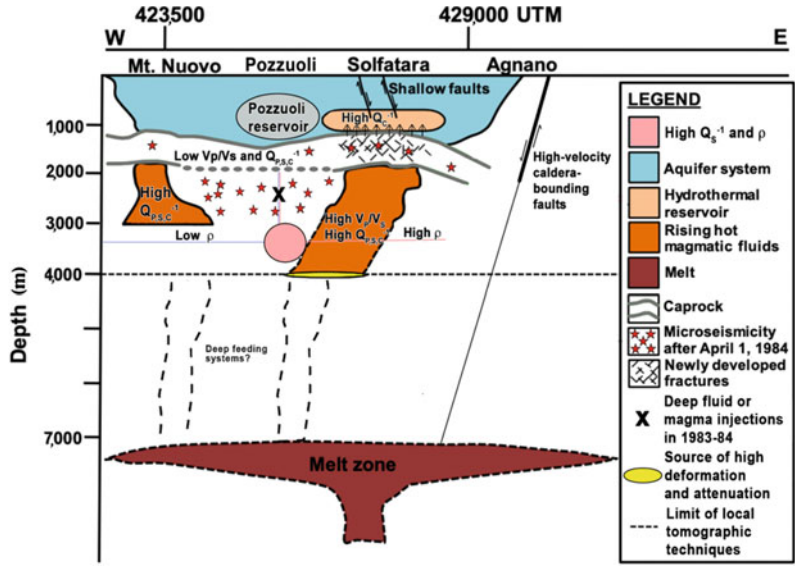

Fig. 21 Schematic illustration of the uppermost crust beneath the Campi Flegrei along an east–west vertical section, based on a joint interpretation of velocity, attenuation, scattering and gravity inversions. Figure modified after Akande et al. (2019)

5 Conclusive Remarks

A review of seismic and gravity data, and tomographic models produced during the past four decades has been here presented in order to give a picture of the structure of the crust beneath the CFc.

The defined lithological and geological discontinuities have been widely depicted, the constraints they give to the definition of magmatic and volcanic processes have been discussed.

The elastic properties of the shallowest 4 km of the upper crust have been reconstructed using velocity tomography elaborated on active and passive seismic data. Information complementary to velocity tomography, improved by seismic attenuation tomography, permit to define lateral lithological changes and the geometry of onshore and offshore fluid and/or small magma bodies (possibly placed during the 1982–1984 bradyseismic crisis) down to 4 km under Pozzuoli town.

Active experiments have permitted to recognise a partially molten body at a depth of ~7.5 km interpreted as an extended magma sill under the caldera.

Acknowledgements This paper has been prepared in the frameworks of the Projects UNREST and V2 (Precursori) funded by the Department of the Civil Protection of Italy and by I.N.G.V, and partially funded by the Spanish research project CGL2011-29499-C02-01, EPHESTOS Istituto Andaluz de Geofisica - Universidad de Granada, Spain.

References

Achauer U, Evans JR, Stauber DA (1988) High-resolution seismic tomography of compressional wave velocity structure at Newberry Volcano, Oregon cascade range. J Geophys Res 93(B9):10135–10147. https://doi.org/10.1029/JB093iB09p10135

AGIP (1987) Modello geotermico del sistema flegreo. Sintesi. Servizi Centrali per l'Esplorazione, SERG-MESG, San Donato Milanese, Italy, 23 pp

Akande WG, De Siena L, Gan Q (2019) Three-dimensional kernel-based coda attenuation imaging of caldera structures controlling the 1982–1984 Campi Flegrei unrest. J Volcanol Geotherm Res 381:273–283

Aki K (1980) Attenuation of shear-waves in the lithosphere for frequencies from 0.05 to 25 Hz. Phys Earth Planet Int 21:50–60

Amoruso A, Crescentini L, Berrino G (2008) Simultaneous inversion of deformation and gravity changes in a horizontally layered half-space: evidences for magma intrusion during the 1982–1984 unrest at Campi Flegrei caldera (Italy). Earth Planet Sci Lett 272(1–2):181–188

Amoruso A, Crescentini L, Sabbetta I (2014) Paired deformation sources of the Campi Flegrei caldera (Italy) required by recent (1980–2010) deformation history. J Geophys Res Solid Earth 119(2):858–879

Aster RC, Meyer RP (1988) Three-dimensional velocity structure and hypocenter distribution in the Campi Flegrei caldera, Italy. Tectonophysics 149:195–218. https://doi.org/10.1016/00401951(88)90173-4

Auger E, Gasparini P, Virieux J, Zollo A (2001) Seismic evidence for an extended magmatic sill under Mt. Vesuvius. Science 294:1510–1512. https://doi.org/10.1126/science.1064893

Auger E, Virieux J, Zollo A (2003) Locating and quantifying the seismic discontinuities in a complex medium through the migration and AVA analysis of reflected and converted waves: an application to the Mt Vesuvius volcano. Geophys J Int 152(2):486–496. https://doi.org/10.1046/j.1365-246X.2003.01864.x

Barberi F, Cassano E, La Torre P, Sbrana A (1991) Structural evolution of Campi Flegrei caldera in light of volcanological and geophysical data. J Volcanol Geotherm Res 48:33–49

Battaglia J, Zollo A, Virieux J, Dello Iacono D (2008) Merging active and passive data sets in travel-time tomography: the case study of Campi Flegrei Caldera (Southern Italy). Geophys Prospect 56:555–573. https://doi.org/10.1111/j.1365-2478.2007.00687.x

Bellucci Sessa E, Castellano M, Ricciolino P (2021) GIS applications in volcano monitoring: the study of seismic swarms at the Campi Flegrei volcanic complex, Italy. Adv Geosci 52:131–144

Benz HM, Chouet BA, Dawson PB, Lahr JC, Page RA, Hole JA (1996) Three-dimensional P and S wave velocity structure of Redoubt Volcano, Alaska. J Geophys Res 101:8111–8128. https://doi.org/10.1029/95JB03046

Berrino G, Corrado G, Riccardi U (1998) Sea gravity data in the Gulf of Naples: a contribution to delineating the structural pattern of the Vesuvian area. J Geophys Res 82:139–150

Berrino G, Corrado G, Riccardi U (2008) Sea gravity data in the Gulf of Naples. A contribution to delineating the structural pattern of the Phlegrean volcanic district. J Volcanol Geotherm Res 175:241–252. https://doi.org/10.1016/j.jvolgeores.2008.03.007

Blacic TM, Latorre D, Virieux J, Vassallo M (2009) Converted phases analysis of the Campi Flegrei caldera using active seismic data. Tectonophysics 470(3–4):243–256. https://doi.org/10.1016/j.tecto.2008.12.006

Bonafede M (1991) Hot fluid migration: An efficient source of round deformation: application to the 1982–1985 crisis at Campi Flegrei-Italy. J Volcanol Geotherm Res 48:187–198

Bonasia V, Del Pezzo E, Pingue F, Scandone R, Scarpa R (1985) Eruptive history, seismic activity and ground deformation at Mt. Vesuvius, Italy. Ann Geofis 3:395–406

Brenguier F, Shapiro NM, Campillo M, Nercessian A, Ferrazzini V (2007) 3-D surface wave tomography of the Piton de la Fournaise volcano using seismic noise correlations. Geophys Res Lett 34:L02305. https://doi.org/10.1029/2006GL028586

Bruno PPG, Cippitelli G, Rapolla A (1998) Seismic study of the Mesozoic carbonate basement around Mt. Somma-Vesuvius, Italy. J Geophys Res 84:311–322. https://doi.org/10.1016/S0377-0273(98)00023-7

Bruno PPG, Rapolla A, Di Fiore V (2003) Structural setting of the Bay of Naples (Italy) seismic reflection data: implications for Campanian volcanism. Tectonophysics 372(3–4):193–213. https://doi.org/10.1016/S0040-1951(03)00327-5

Caliro S, Chiodini G, Moretti R, Avino R, Granieri D, Russo M, Fiebig J (2007) The origin of the fumaroles of La Solfatara (Campi Flegrei, South Italy). Geochim Cosmochim Acta 71:3040–3055. https://doi.org/10.1016/j.gca.2007.04.007

Calò M, Tramelli A (2018) Anatomy of the campi flegrei caldera using enhanced seismic tomography models. Sci Rep 8(1):1–12

Campos-Enriquez JO, Arredondo-Fragoso JJ (1992) Gravity study of Los Humeros caldera complex, Mexico: structure and associated geothermal system. J Volcanol Geotherm Res 49(1–2):69–90

Capuano P, Achauer U (2003) Gravity field modeling in the Vesuvius and Campanian area. In: Zollo A et al. (eds) The TomoVes seismic project: looking inside Mt. Vesuvius. Cuen, Naples, Italy

Capuano P, Russo G, Vanorio T, Prevete R, Auger E, Bonagura M, Caielli G, Convertito V, Damiano N, D'Auria L, Emolo A, Lovisa L, Moretti M (2006) 1984 Campi Flegrei seismic waveforms compilation. In: Zollo A et al. (eds) Geophysical exploration of the Campi Flegrei (Southern Italy) Caldera' interiors: data, methods and results. Doppiavoce, Naples, Italy, pp 15–24. ISBN: 88-89972-04-1

Capuano P, Russo G, Civetta L, Orsi G, D'Antonio M, Moretti R (2013) The active portion of the Campi Flegrei caldera structure imaged by 3D inversion of gravity data. Geochem Geophys Geosyst 14:4681–4697

Carlino S, Somma R (2009) Eruptive versus non-eruptive behaviour of large calderas: the example of Campi Flegrei caldera (Southern Italy). Bull Volcanol 72 (7):871–886. https://doi.org/10.1007/s00445-010-0370-y

Casertano L, Oliveri A, Quagliariello MT (1976) Hydrodynamics and geodynamics in the Phlegraean Fields area of Italy. Nature 264:161–164

Cassano E, La Torre P (1987) Geophysics. In: Rosi M, Sbrana A (eds) Phlegrean Fields. Quaderni de "La Ricerca Scientifica", vol 114(9). CNR, Rome, Italy, pp 94–103

Chiarabba C, Moretti M (2006) An insight into the unrest phenomena at the Campi Flegrei caldera from V_P and V_P/V_S tomography. Terra Nova 18:373–379. https://doi.org/10.1111/j.1365-3121.2006.00701.x

Chiodini G, Todesco M, Caliro S, Del Gaudio C, Macedonio G, Russo M (2003) Magma degassing as a trigger of bradyseismic events: the case of Phlegrean Fields (Italy). Geophys Res Lett 30(8):1434. https://doi.org/10.1029/2002GL016790

Chiodini G, Paonita A, Aiuppa A, Costa A, Caliro S, De Martino P, Acocella V, Vandemeulebrouck J (2016) Magmas near the critical degassing pressure drive volcanic unrest towards a critical state. Nat Commun 7 (1):1–9

Chiodini G, Caliro S, Avino R, Bini G, Giudicepietro F, De Cesare W, Ricciolino P, Aiuppa A, Cardellini C, Petrillo Z, Selva J, Siniscalchi A, Tripaldi S (2021) Hydrothermal pressure-temperature control on CO_2 emissions and seismicity at Campi Flegrei (Italy). J Volcanol Geotherm Res 414:107245

Chouet B (1988) Resonance of a fluid-driven crack: radiation properties and implications for the source of long-period events and harmonic tremor. J Geophys Res 93(B5):4375–4400. https://doi.org/10.1029/JB093iB05p04375

Chu R, Helmberger DV, Sun D, Jackson JM, Zhu L (2010) Mushy magma beneath Yellowstone. Geophys Res Lett 37:L01306. https://doi.org/10.1029/2009GL041656

Cinque A, Rolandi G, Zamparelli V (1985) L'estensione dei depositi marini olocenici nei Campi Flegrei in relazione alla vulcano-tettonica. Boll Soc Geol It 104 (2):327–348

Cinque A, Patacca E, Scandone P, Tozzi M (1993) Quaternary kinematic evolution of the Southern Apennines. Relationships between surface geological features and deep lithospheric structures. Ann Geophys 36:249–260

Davy BW, Caldwell TG (1998) Gravity, magnetic and seismic surveys of the caldera complex, Lake Taupo, North Island, New Zealand. J Volcanol Geotherm Res 81:69–89

De Bonitatibus A, Latmiral G, Mirabile L, Palumbo A, Sarpi E, Scalera A (1970) Rilievi sismici per riflessione: strutturali, ecografici (fumarole) e batimetrici del Golfo di Pozzuoli. Boll Soc Natur Napoli Italy 79:97–115

De Landro G, Serlenga V, Russo G, Amoroso O, Festa G, Bruno PP, Gresse M, Vandemeulebrouck J, Zollo A (2017) 3D ultra-high resolution seismic imaging of shallow Solfatara crater in Campi Flegrei (Italy): new Insights on deep hydrothermal fluid circulation processes. Sci Reports 7(1). https://doi.org/10.1038/s41598-017-03604-0

de Lorenzo S, Zollo A, Monelli F (2001) Source parameters and three-dimensional attenuation structure from the inversion of microearthquake pulse width data: Qp imaging and inferences on the thermal state

of Campi Flegrei caldera (Southern Italy). J Geophys Res 106. https://doi.org/10.1029/2000JB900462

De Siena L, Del Pezzo E, Bianco F, Tramelli A (2009) Multiple resolution seismic attenuation imaging at Mt Vesuvius. Phys Earth Planet Inter 173:17–32

De Siena L, Del Pezzo E, Bianco F (2010) Seismic attenuation imaging of Campi Flegrei: evidence of gas reservoirs, hydrothermal basins, and feeding systems. J Geophys Res 115:B09312. https://doi.org/10.1029/2009JB006938

De Siena L, Del Pezzo E, Bianco F (2011) A scattering image of Campi Flegrei from the auto correlation functions of velocity tomograms. Geophys J Int 184 (3):1304–1310. https://doi.org/10.1111/j.1365-246X.2010.04911.x

De Siena L, Thomas C, Aster R (2014a) Multi-scale reasonable attenuation tomography analysis (MuRAT): an imaging algorithm designed for volcanic regions. J Volcanol Geotherm Res 277:22–35

De Siena L, Thomas C, Waite GP, Moran SC, Klemme S (2014b) Attenuation and scattering tomography of the deep plumbing system of Mount St. Helens. J Geophys Res Solid Earth 119(11):8223–8238

De Siena L, Amoruso A, Del Pezzo E, Wakeford Z, Castellano M, Crescentini L (2017a) Space-weighted seismic attenuation mapping of the aseismic source of Campi Flegrei 1983–1984 unrest. Geophys Res Lett 44(4):1740–1748

De Siena L, Chiodini G, Vilardo G, Del Pezzo E, Castellano M, Colombelli S, Tisato N, Ventura G (2017b) Source and dynamics of a volcanic caldera unrest: Campi Flegrei, 1983–1984. Sci Rep 7(1):1–13

De Siena L, Sammarco C, Cornwell DG, La Rocca M, Bianco F, Zaccarelli L, Nakahara H (2018) Ambient seismic noise image of the structurally controlled heat and fluid feeder pathway at Campi Flegrei caldera. Geophys Res Lett 45(13):6428–6436

Del Pezzo E, Bianco F, De Siena L, Zollo A (2006) Small scale shallow attenuation structure at Mt. Vesuvius, Italy. Phys Earth Planet Inter 157:257–268

Del Pezzo E, Bianco F (2013a) A reappraisal of seismic Q evaluated in Campi Flegrei caldera. Receipt for the application to risk analysis. J Seismol 17:829–837. https://doi.org/10.1007/s10950-012-9349-9

Del Pezzo E, Bianco F (2013b) Inside Mt. Vesuvius, a new method to look at the seismic tomographic imaging. Ann Geophys 56(4):S0443. ISSN: 2037-416X. https://doi.org/10.4401/ag-6449

Del Pezzo E, Ibanez J, Prudencio J, Bianco F, De Siena L (2016) Absorption and scattering 2-D volcano images from numerically calculated space-weighting functions. Geophys J Int 206(2):742–756

Dello Iacono D, Zollo A, Vassallo M, Vanorio T, Judenherc S (2009) Seismic images and rock properties of the very shallow structure of Campi Flegrei caldera (Southern Italy). Bull Volcanol 71(3):275–284. https://doi.org/10.1007/s00445-008-0222-1

DeNosaquo KR, Smith RB, Lowry AR (2009) Density and lithospheric strength models of the Yellowstone-Snake River Plain volcanic system from gravity and heat flow data. J Volcanol Geotherm Res 188:108–127. https://doi.org/10.1016/j.jvolgeores.2009.08.006

Di Stefano R, Bianchi I, Ciaccio MG, Carrara G, Kissling E (2011) Three-dimensional Moho topography in Italy: new constraints from receiver functions and controlled source seismology. Geochem Geophys Geosys 12:Q09006. https://doi.org/10.1029/2011GC003649

Di Vito MA, Isaia R, Orsi G, Southon J, de Vita S, D'Antonio M, Pappalardo L, Piochi M (1999) Volcanism and deformation since 12,000 years at the Campi Flegrei caldera (Italy). J Volcanol Geotherm Res 91:221–246

Di Vito MA, Acocella V, Aiello G, Barra D, Battaglia M, Carandente A, Del Gaudio C, de Vita S, Ricciardi GP, Ricco C, Scandone R, Terrasi F (2016) Magma transfer at Campi Flegrei caldera (Italy) before the 1538 AD eruption. Sci Rep 6:32245. https://doi.org/10.1038/srep32245

Dvorkin J, Prasad M, Sakai A, Lavoie D (1999) Elasticity of marine sediments: rock physics modeling. Geophys Res Lett 26(12):1781–1784. https://doi.org/10.1029/1999GL900332

Eberhart-Phillips D, Reyners M, Chadwick M, Chiu JM (2005) Crustal heterogeneity and subduction processes: 3-D Vp, Vp/Vs and Q in the southern North Island, New Zealand. Geophys J Int 162(1):270–288

Fedi M, Nunziata C, Rapolla A (1991) The Campania-Campi Flegrei area: a contribution to discern the best structural model from gravity interpretation. J Volcanol Geotherm Res 48:51–59

Fedi M, Cella F, D'Antonio M, Florio G, Paoletti V, Morra V (2018) Gravity modeling finds a large magma body in the deep crust below the Gulf of Naples, Italy. Sci Rep 8:8229. https://doi.org/10.1038/s41598-018-26346-z

Ferrazzini V, Aki K (1987) Slow waves trapped in a fluid-filled infinite crack: implication for volcanic tremor. J Geophys Res 92(B9):9215–9223. https://doi.org/10.1029/JB092iB09p09215

Ferrucci F, Gaudiosi G, Pino NA, Luongo G, Hirn A, Mirabile L (1989) Seismic detection of a major Moho upheaval beneath the Campania volcanic area (Naples, Southern Italy). Geophys Res Lett 16(11):1317–1320. https://doi.org/10.1029/GL016i011p01317

Ferrucci F, Hirn A, De Natale G, Virieux J, Mirabile L (1992) P-SV conversions at a shallow boundary beneath Campi Flegrei caldera (Italy): evidence for the magma chamber. J Geophys Res 97(B11):15351–15359. https://doi.org/10.1029/92JB00888

Fialko Y, Simons M, Khazan Y (2001) Finite source modelling of magmatic unrest in Socorro, New Mexico, and Long Valley, California. Geophys J Int 146:191–200. https://doi.org/10.1046/j.1365-246X.2001.00453.x

Finetti I, Morelli C (1974) Esplorazione sismica a riflessione nei Golfi di Napoli e Pozzuoli. Boll Geofis Teor Appl 16:175–222

Florio G, Fedi M, Cella F, Rapolla A (1999) The Campanian Plain and Phlegrean Fields: structural

setting from potential field data. J Volcanol Geotherm Res 91:361–379

Fournier N, Rymer H, Williams-Jones G, Brenes J (2004) High-resolution gravity survey: investigation of subsurface structures at Poas volcano, Costa Rica. Geophys Res Lett 31:L15602. https://doi.org/10.1029/2004GL020563

Gaeta FS, De Natale G, Peluso F, Castagnolo D, Troise C, Pingue F, Mita DG, Rossano S (1998) Genesis and evolution of unrest episodes at Campi Flegrei caldera: the role of the thermal fluid dynamical processes in the geothermal system. J Geophys Res 103:20921–20933

Gailler LS, Lénat JF, Lambert M, Levieux G, Villeneuve N, Froger JL (2009) Gravity structure of Piton de la Fournaise volcano and inferred mass transfer during the 2007 crisis. J Volcanol Geotherm Res 184(1–2):31–48. https://doi.org/10.1016/j.jvolgeores.2009.01.024

Gasparini P and TomoVes Working Group (1998) Looking inside Mount Vesuvius. EOS Trans Am Geophys Un 79(19):229–232

De Gori P, Chiarabba C, Patanè D (2005) Qp structure of Mount Etna: constraints for the physics of the plumbing system. J Geophys Res Solid Earth 110(B5)

Hansen S, Thurber C, Mandernach M, Haslinger F, Doran C (2004) Seismic velocity and attenuation structure of the east rift zone and south flank of Kilauea Volcano, Hawaii. Bull Seismol Soc Am 94 (4):1430–1440

Hashin Z, Shtrikman S (1963) A variational approach to the elastic behavior of multiphase minerals. J Mech Phys Solids 11(2):127–140. https://doi.org/10.1016/0022-5096(63)90060-7

Hellweg M (2000) Physical models for the source of Lascar's harmonic tremor. J Volcan Geotherm Res 101(1–2):83–198

Hobro JW, Singh SC, Minshull TA (2003) Three-dimensional tomographic inversion of combined reflection and refraction seismic traveltime data. Geophys J Int 152(1):79–93. https://doi.org/10.1046/j.1365-246X.2003.01822.x

Hole JA (1992) Nonlinear high-resolution three-dimensional seismic travel time tomography. J Geophys Res 97(B5):6553–6562. https://doi.org/10.1029/92JB00235

Huffman A, Castagna J (2001) The petrophysical basis for shallow water flow prediction using multicomponent seismic data. Lead Edge 20(9):1030–1052

Imbò G, Bonasia V, Gasparini P (1964) Rilievo gravimetrico dell'isola di Procida. Ann Oss Ves, Naples, Italy 6:117–138

Jolivet L, Faccenna C, Piromallo C (2009) From mantle to crust: Stretching the Mediterranean. Earth and Planetary Science Letters 285(1–2):198–209. https://doi.org/10.1016/j.epsl.2009.06.017

Jousset P, Neuberg J, Sturton S (2003) Modelling the time-dependent frequency content of low-frequency volcanic earthquakes. J Volcanol Geotherm Res 128:201–223

Judenherc S, Zollo A (2004) The Bay of Naples (southern Italy): constraints on the volcanic structures inferred from a dense seismic survey. J Geophys Res 109 (B10):B10312. https://doi.org/10.1029/2003JB002876

Latorre D, Virieux J, Monfret T, Monteiller V, Vanorio T, Got JL, Lyon-Caen H (2004) A new seismic tomography of Aigion area (Gulf of Corinth-Greece) from a 1991 dataset. Geophys J Int 159:1013–1031

Locke CA, Cassidy J, MacDonald A (1993) Three-dimensional structure of relict stratovolcanoes in Taranaki, New Zealand: evidence from gravity data. J Volcanol Geotherm Res 59(1–2):121–130. https://doi.org/10.1016/0377-0273(93)90081-2

Lomax A, Zollo A, Capuano P, Virieux J (2001) Precise, absolute earthquake location under Somma Vesuvius volcano using a new three dimensional velocity model. Geophys J Int 146:313–331

Maercklin N (2008) Seismic scatterer imaging using shot array beamforming: method and application to the Campi Flegrei caldera. In: Marzocchi W, Zollo A (eds) Conception, verification, and application of innovative techniques to study active volcanoes. Doppiavoce, Naples, Italy, pp 261–268. ISBN: 978-88-89972-09-0

Maercklin N, Zollo A (2009) Estimation of elastic contrasts in a layered model from seismic PS-to-PP amplitude ratios. Geophys J Int 179(3):1617–1626. https://doi.org/10.1111/j.1365-246X.2009.04350.x

Maino A, Tribalto G (1971) Rilevamento gravimetrico di dettaglio dell'isola d'Ischia, Napoli. Boll Serv Geol Ital 92:109–122

Malone SD, Boyko C, Weaver CS (1983) Seismic precursors to the Mount St. Helens eruptions in 1981 and 1982. Science 221(4618):1376–1378

Mangiacapra A, Moretti R, Rutherford M, Civetta L, Orsi G, Papale P (2008) The deep magmatic system of the Campi Flegrei caldera (Italy). Geophys Res Lett 35:L21304. https://doi.org/10.1029/2008GL035550

Masturyono, McCaffrey R, Wark DA, Roecker SW, Fauzi, Ibrahim G, Sukhyar (2001) Distribution of magma beneath Toba caldera complex, north Sumatra, Indonesia, constrained by three-dimensional P wave velocities, seismicity, and gravity. Geochem Geophys Geosyst 2. https://doi.org/10.1029/2000GC000096

Mavko G, Mukerji T, Dvorkin J (1998) The rock physics handbook: tools for seismic analysis in porous media. Cambridge University Press, Cambridge, UK

Milia A, Torrente M (2003) Late-quaternary volcanism and transtensional tectonics in the Bay of Naples, Campanian continental margin, Italy. Miner Petrol 79:49–65

Monteiller V, Got JL, Virieux J, Okubo P (2005) An efficient algorithm for double-difference tomography and location in heterogeneous media, with an application to the Kilauea volcano. J Geophys Res 110: B12306. https://doi.org/10.1029/2004JB003466

Mora MM, Lesage P, Valette B, Alvarado GE, Leandro C, Metaxian JP, Dorel J (2006) Shallow velocity structure and seismic site effects at Arenal volcano, Costa

Rica. J Volcanol Geotherm Res 152(1–2):121–139. https://doi.org/10.1016/j.jvolgeores.2005.09.013
Moretti R, Arienzo I, Civetta L, Orsi G, Papale P (2013) Multiple magma degassing sources at an explosive volcano. Earth Planet Sci Lett 367:95–104. https://doi.org/10.1016/j.epsl.2013.02.013
Moretti R, De Natale G, Troise C (2020) Hydrothermal versus magmatic: geochemical views and clues into the unrest dilemma at Campi Flegrei. In: Vesuvius, Campi Flegrei, and Campanian volcanism. Elsevier, pp 371–406
Murase T, McBirney AR (1973) Properties of some common igneous rocks and their melt at high temperatures. Geol Soc Am Bull 84(11):3563–3592
Nakajima J, Hasegawa A (2003) Tomographic imaging of seismic velocity structure in and around the Onikobe volcanic area, northeastern Japan: implications for fluid distribution. J Volcanol Geother Res 127(1–2):1–18
Nakamichi H, Tanaka S, Hamaguchi H (2002) Fine S wave velocity structure beneath Iwate volcano, northeastern Japan, as derived from receiver functions and travel times. J Volcanol Geotherm Res 116(3–4):235–255. https://doi.org/10.1016/S0377-0273(02)00218-4
Nercessian A, Hirn A, Tarantola A (1984) Three dimensional seismic transmission prospecting of the Mont Dore volcano, France. Geophys J R Astr Soc 76:307–315
Neuberg J, Luckett, Ripepe M, Braun T (1994) Highlight from a seismic broadband array on Stromboli volcano. Geophys Res Lett 21:749–752
Neuberg JW, Tuffen H, Collier L, Green D, Powell T, Dingwell D (2006) The trigger mechanism of low-frequency earthquakes on Montserrat. J Volcanol Geotherm Res 153(1–2):37–50. https://doi.org/10.1016/j.jvolgeores.2005.08.008
Nishigami KY (1991) A new inversion method of coda waveforms to determine spatial distribution of coda scatterers in the crust and uppermost mantle. Geophys Res Lett 18(12):2225–2228
Nunziata C, Costanzo M (2010) Low Vs crustal zones in the Campanian plain (Southern Italy). Miner Petrol 100(3):215–225. https://doi.org/10.1007/s00710-010-0129-3
Nur A, Marion D, Yin H (1991) Wave velocities in sediments. In: Hovem J, Richardson MD, Stoll RD (eds) Shear waves in marine sediments. Kluwer Academic, pp 131–140
Nur A, Mavko G, Dvorkin J, Galmundi D (1995) Critical porosity: the key to relating physical properties to porosity in rocks. In: Proceedings of 65th annual international meeting social expl and geophysics, p 878
Oliveri del Castillo A, Quagliariello MT (1969) Sulla genesi del bradisismo flegreo. Atti Assoc Geofis Ital 4:1–4
Operto S, Ravaut C, Improta L, Virieux J, Herrero A, Dell'Aversana P (2004) Quantitative imaging of complex structures from dense wide-aperture seismic data by multiscale traveltime and waveform inversions: a case study. Geophys Prosp 52:625–651. https://doi.org/10.1111/j.1365-2478.2004.00452.x
Orsi G, D'Antonio M, de Vita S, Gallo G (1992) The Neapolitan Yellow Tuff, a large-magnitude trachytic phreatoplinian eruption: eruptive dynamics, magma withdrawal and caldera collapse. J Volcanol Geotherm Res 53:275–287. https://doi.org/10.1016/0377-0273(92)90086-S
Orsi G, de Vita S, Di Vito M (1996) The restless, resurgent Campi Flegrei nested caldera (Italy): constraints on its evolution and configuration. J Volcanol Geotherm Res 74:179–214
Orsi G, Civetta L, Del Gaudio C, de Vita S, Di Vito MA, Isaia R, Petrazzuoli SM, Ricciardi G, Ricco C (1999) Short-term ground deformations and seismicity in the resurgent Campi Flegrei caldera (Italy): an example of active block-resurgence in a densely populated area. J Volcanol Geotherm Res 91(2–4):415–451
Orsi G, De Vita S, Di Vito M, Isaia R, Nave R, Heiken, G (2003) Facing volcanic and related hazards in the neapolitan area. In: Heiken G, Fakuntiny R, Sutter J (eds) Earth science in the city: a reader, vol 56. Wiley
Orsi G, Di Vito MA, Isaia R (2004) Volcanic hazard assessment at the restless Campi Flegrei caldera. Bull Volcanol 66:514–530. https://doi.org/10.1007/s00445-003-0336-4
Pappalardo L, Matrolorenzo G (2012a) Rapid differentiation in a sill-like magma reservoir: a case study from the Campi Flegrei caldera. Sci Rep 2(712). https://doi.org/10.1038/srep00712
Pappalardo L, Mastrolorenzo G (2012b) Rapid differentiation in a sill-like magma reservoir: a case study from the Campi Flegrei caldera. Sci Rep 2:712. https://doi.org/10.1038/srep00712
Patacca E, Sartori R, Scandone P (1990) Tyrrhenian basin and apenninic arcs: kinematic relations since late Tortonian times. Mem Soc Geol It 45:425–451
Patanè D, Barberi G, Cocina O, De Gori P, Chiarabba C (2006) Time-resolved seismic tomography detects magma intrusions at Mount Etna. Science 313 (5788):821–823. https://doi.org/10.1126/science.1127724
Pepe S, De Siena L, Barone A, Castaldo R, D'Auria L, Manzo M, Casu F, Fedi M, Lanari R, Bianco F, Tizzani P (2019) Volcanic structures investigation through SAR and seismic interferometric methods: the 2011–2013 Campi Flegrei unrest episode. Remote Sens Environ 234(111440)
Pescatore T, Diplomatico G, Senatore MR, Tramutoli M, Mirabile L (1984) Contributi allo studio del Golfo di Pozzuoli: aspetti stratigrafici e strutturali. Mem Soc Geol Ital 27:133–149
Prudencio J, De Siena L, Ibáñez JM, Del Pezzo E, Garcia-Yeguas A, Diaz-Moreno A (2015) The 3D attenuation structure of deception island (Antarctica). Surv Geophys 36(3):371–390
Rawlinson N, Sambridge M (2004) Wave front evolution in strongly heterogeneous layered media using the fast marching method. Geophys J Int 156(3):631–647

Rosi M, Sbrana A (eds) (1987) Phlegrean Fields. Quad Ric Sci 114(9):1–175. ISSN: 0556-9664

Rosi M, Sbrana A, Principe C (1983) The phlegrean fields: structural evolution, volcanic history and eruptive mechanisms. J Volcanol Geoth Res 17(1–4):273–288

Rowe CA, Aster RC, Kyle PR, Schlue JW (1998) RR dibble broadband recording of strombolian explosions and associated very-longperiod seismic signals on Mount Erebus Volcano, Ross Island, Antarctica. Geophys Res Lett 25(13):2297–2300

Rowe CA, Aster RC, Kyle PR, RR Dibble, Schlue JW (2000) Seismic and acoustic observations at Mount Erebus volcano, Ross island, Antarctica, 1994–1998. J Volcanol Geotherm Res 101(1–2):105–128

Rymer H (1994) Microgravity change as a precursor to volcanic activity. J Volcanol Geotherm Res 61:311–328

Sacchi M, Alessio G, Aquino I, Esposito E, Molisso F, Nappi R, Porfido S, Violante C (2009) Risultati preliminari della campagna oceanografica CAFE_07—Leg 3 nei Golfi di Napoli e Pozzuoli, Mar Tirreno Orientale. Quad Geofis 64:1–28. ISSN: 1590-2595

Sanders CO, Ponko SC, Nixon LD, Schwartz FA (1995) Seismological evidence for magmatic and hydrothermal structure in Long Valley caldera from local earthquake attenuation and velocity tomography. J Geophys Res 100:8311–8326

Sato H, Fehler MC, Maeda T (2012) Seismic wave propagation and scattering in the heterogeneous earth, vol 496. Springer, Berlin, Germany

Satriano C, Zollo A, Rowe C (2008) Iterative tomographic analysis based on automatic refined picking. Geophys Pros 56:467–475. https://doi.org/10.1111/j.1365-2478.2008.00700.x

Schimmel M, Paulssen H (1997) Noise reduction and detection of weak, coherent signals through phase-weighted stacks. Geophys J Int 130(2):497–505

Schmeling H (1985) Numerical models on the influence of partial melt on elastic, anelastic and electric properties of rocks. Part I: elasticity and an elasticity. Phys Earth Planet Int 41(1):34–57

Schurr B, Asch G, Rietbrock A, Trumbull R, Haberland C (2003) Complex patterns of fluid and melt transport in the central Andean subduction zone revealed by attenuation tomography. Earth Planet Sci Lett 215 (1–2):105–119

Serlenga V, de Lorenzo S, Russo G, Amoroso O, Garambois S, Virieux J, Zollo A (2016) A three-dimensional QP imaging of the shallowest subsurface of Campi Flegrei offshore caldera, Southern Italy. Geophys Res Lett 43(21):11209–11218

Siniscalchi A, Tripaldi S, Romano G, Chiodini G, Improta L, Petrillo Z, D'Auria L, Caliro S, Avino R (2019) Reservoir structure and hydraulic properties of the Campi Flegrei geothermal system inferred by audiomagnetotelluric, geochemical, and seismicity study. J Geophys Res Solid Earth 124(6):5336–5356

Sketsiou P, Napolitano F, Zenonos A, De Siena L (2020) New insights into seismic absorption imaging. Phys Earth Planet Int 298:106337

Stabile TA, Zollo A, Vassallo M, Iannaccone G (2007) Underwater acoustic channel properties in the Gulf of Naples and their effects on digital data transmission. Ann Geophys 50:313–328

Takei Y (2002) Effect of pore geometry on VP/VS: from equilibrium geometry to crack. J Geophys Res Solid Earth 107(B2):ECV-6

Thorpe S, Locke CA, Brown GC, Francis PW, Randal M (1981) Magma chamber below Poàs volcano, Costa Rica. J Geol Soc 138:367–373. https://doi.org/10.1144/gsjgs.138.3.0367

Thurber CH (1984) Seismic detection of the summit magma complex of Kilauea volcano, Hawaii. Science 223:165–167

Todesco M, Chiodini G, Macedonio G (2003) Monitoring and modeling hydrothermal fluid emission at La Solfatara (Phlegrean Fields, Italy). An interdisciplinary approach to the study of diffuse degassing. J Volcanol Geotherm Res 125:57–79. https://doi.org/10.1016/S0377-0273(03)00089-1

Tramelli A, Del Pezzo E, Bianco F, Boschi E (2006) 3-D scattering image of the Campi Flegrei caldera (Southern Italy). New hints on the position of the old caldera rim. Phys Earth Planet Int 155:269–280

Tramelli A, Del Pezzo E, Fehler MC (2009) 3-D scattering image of Mt. Vesuvius. Bull Seismol Soc Am 99(3):1962–1972. https://doi.org/10.1785/0120080273

Vanorio T, Kanitpanyacharoen W (2015) Rock physics of fibrous rocks akin to Roman concrete explains uplifts at Campi Flegrei caldera. Science 349(6248):617–621. https://doi.org/10.1126/science.aab1292

Vanorio T, Virieux J, Capuano P, Russo G (2005) Three-dimensional seismic tomography from P wave and S wave microearthquake travel times and rock physics characterization of the Campi Flegrei caldera. J Geophys Res 110(B3):B03201. https://doi.org/10.1029/2004JB003102

Vassallo M, Zollo A, Dello Iacono D, Maercklin N, Virieux J (2008) Converted phase identification and retrieval of Vp/Vs ratios from move-out reflection analysis: application to the Campi Flegrei caldera. In: Marzocchi W, Zollo A (eds) Conception, verification, and application of innovative techniques to study active volcanoes. Doppiavoce, Naples, Italy, pp 349–360

Vassallo M, Zollo A, Festa G, Maercklin N (2010) Campi Flegrei (Southern Italy) calderic model from the joint inversion of reflected (PP, PS) and first arrival seismic traveltimes. 7th EGU General assembly geophysics research abstract 12:13157

Vilardo G, Isaia R, Ventura G, De Martino P, Terranova C (2010) InSAR permanent scatterer analysis reveals fault re-activation during inflation and deflation episodes at Campi Flegrei caldera. Remote Sens Environ 114(10):2373–2383

Vitale S, Isaia R (2014) Fractures and faults in volcanic rocks (Campi Flegrei, Southern Italy): insight into volcano-tectonic processes. Int J Earth Sci 103 (3):801–819

Yokoyama I (1989) Microgravity and height changes caused by volcanic activity: four Japanese examples. Bull Volcanol 51:333–345

Yokoyama S, Mena M (1991) Structure of La Primavera caldera, Jalisco, Mexico. J Volcanol Geotherm Res 47:183–194

Young N, Isaia R, Gottsmann J (2020) Gravimetric constraints on the hydrothermal system of the Campi Flegrei caldera. J Geophys Res Solid Earth 125(7): e2019JB019231

Zhdanov MS (2002) Geophysical inverse theory and regularization problems. Elsevier, Amsterdam, The Netherlands, p 605

Zimmer M (2003) Controls on the seismic velocities of unconsolidated sands: measurements of pressure, porosity and compaction effects. Ph.D. thesis, Stanford University, Stanford, CA

Zollo A, Judenherc S, Auger E, D'Auria L, Virieux J, Capuano P, Chiarabba C, De Franco R, Makris J, Michelini A, Musacchio G (2003) Evidence for the buried rim of Campi Flegrei caldera from 3-D active seismic imaging. Geophys Res Lett 30(19). https://doi.org/10.1029/2003GL018173

Zollo A, Maercklin N, Vassallo M, Dello Iacono D, Virieux J, Gasparini P (2008) Seismic reflections reveal a massive melt layer feeding Campi Flegrei caldera. Geophys Res Lett 35(12):L12306. https://doi.org/10.1029/2008GL034242